Astron. Astrophys. 321, 531–548 (1997)

ASTRONOMY AND ASTROPHYSICS

Quantitative analysis of the FUV, UV and optical spectrum of the O3 star HD 93129A⋆,⋆⋆

G. Taresch[1], R.P. Kudritzki[1,2], M. Hurwitz[3], S. Bowyer[3,4], A.W.A. Pauldrach[1], J. Puls[1], K. Butler[1], D.J. Lennon[1,2], and S.M. Haser[1]

[1] Institut für Astronomie und Astrophysik der Universität München, Scheinerstr. 1, D-81679 München, Germany
[2] Max-Planck-Institut für Astrophysik, D-85740 Garching bei München, Germany
[3] Space Sciences Laboratory, University of California, Berkeley, California, USA
[4] Astronomy Department, University of California, Berkeley, California, USA

Received 17 June 1996 / Accepted 16 August 1996

Abstract. A quantitative analysis of the extremely hot and massive galactic O3 If* supergiant HD 93129A is carried out using stellar wind and pseudo photospheric lines observed in the FUV, UV and optical spectrum together with hydrodynamical NLTE model atmospheres. The analysis in the FUV is combined with spectrum synthesis of the molecular and atomic/ionic interstellar spectrum to disentangle stellar and interstellar blends. It is demonstrated that the combined stellar/interstellar spectrum synthesis technique is crucial for the determination of both interstellar column densities and stellar properties.

The fraction of hydrogen atoms in molecular form in the Carina interstellar clouds is found to be 0.1, smaller than one would expect for its E(B-V) value of 0.54. We attribute this to dissociation by the strong FUV radiation field of HD 93129A. The excitation temperature of ortho-hydrogen (J=1) is about 80K, whereas the excitation to higher levels requires temperatures up to 230 K in accordance with NLTE effects for interstellar H_2 as discussed in the literature. The abundance of HD relative to H_2 is of the order of 10^{-5}. For CO we obtain an upper limit of 2.6×10^{-5}. Abundances for the interstellar atomic and ionic species are also derived.

The terminal velocity of the stellar wind of HD 93129A is 3200 ± 200 km/s and the rate of mass-loss is $18\times10^{-6}\ M_\odot$/yr. The ionization equilibrium of the optical emission and P-Cygni lines of N III, N IV and N V is used to determine the effective temperature as $T_{\rm eff}$=52000±1000 K in reasonable agreement with previous values obtained from the helium ionization equilibrium. This high temperature is confirmed independently by an analysis of the Ar VI/Ar VII ionization equilibrium in the FUV. The luminosity of HD 93129A is log $L/L_\odot$=6.4±0.1 corresponding to a zero age main sequence mass of slightly in excess of 120 $M_\odot$. This very high mass is consistent with the mass determined from the stellar gravity and with the mass derived from V_∞ using the theory of radiation driven winds. HD 93129A is thus the most luminous and most massive star known in our galaxy. The abundance determinations yield clear evidence of contamination with CNO-cycled matter in the atmosphere. The abundances of heavier elements are about solar. The presence of high ionization stages such as O VI can be explained by X-ray emission due to stellar wind shocks of low temperature (2.5×10^6 K) corresponding to the jump velocity of 500 km/s obtained from UV and FUV P-Cygni profiles. Their luminosity is 1.6 dex smaller than the luminosity of the high temperature shocks (1.1×10^7 K) observed directly with the ROSAT PSPC. Using effective temperature, gravity, radius and abundances as input parameters we calculate radiation driven wind models for HD 93129A. We find that the theory is able to reproduce the extreme stellar wind properties very precisely.

Key words: stars: atmospheres – stars: fundamental parameter – stars: individual: HD93129A – ISM: abundances – ISM: molecules – X-rays: stars

1. Introduction

The Carina nebula, NGC 3372, and its very young stellar clusters, Trumpler 14 and 16, contain a remarkable concentration of massive and luminous stars. Among these, the most spectacular objects - besides the enigmatic η Carina - are the two O3 stars HD 93250 and HD 93129A. With masses of about 100 $M_\odot$ and luminosities clearly in excess of $10^6\ L_\odot$, they are the most massive and most luminous stars in our galaxy (Kudritzki 1980, Kudritzki 1992, Puls et al. 1996, Simon et al. 1983).

Send offprint requests to: G. Taresch

⋆ Based on the development and utilization of ORFEUS (Orbiting and Retrievable Far and Extreme Ultraviolet Spectrometers), a collaboration of the Astronomical Institute of the University of Tuebingen, the Space Astrophysics Group, University of California, Berkeley, and the Landessternwarte Heidelberg

⋆⋆ Tables 3-6 are only available in electronic form at http://cdsweb.u-strasbg.fr/abstract.html

These conclusions based upon NLTE analysis of the hydrogen and helium optical spectra, yielding effective temperature (T_{eff}=50500K), stellar radius (R_*=20$R_\odot$), gravity ($logg$=3.95) and helium abundance (N(He)/N(H)=0.1). Additional evidence for the extreme nature of these objects comes from the terminal velocity (V_∞) of the stellar wind, determined from the N V and C IV UV resonance lines, which for radiation driven winds is a strong function of the stellar mass.

So far the information contained in UV and optical metal lines of these objects has not been used for quantitative spectroscopic studies based on NLTE model atmospheres, mostly because brief inspection of the spectra already indicates that these lines are affected by the presence of strong stellar winds. The study presented here is the first attempt to analyze the FUV, UV and optical metal lines quantitatively with the goal of determining stellar abundances and independent information about the crucial stellar parameters and the physical conditions in the dense stellar winds of these objects. It was triggered by the success of the ORFEUS mission which provided FUV spectroscopic data for both HD 93129A and HD 93250 for the first time. This allows a detailed investigation similar to that of Pauldrach et al. ((1994), hereafter PKPBH) who analyzed FUV and UV Copernicus and IUE spectra of the nearby O-star ζ Puppis.

In this paper, we concentrate on HD 93129A, which from its spectral appearance is much more spectacular than HD 93250. The latter is a main sequence star classified as O3 V ((f)) with very weak emission features, whereas the former is an extreme supergiant classified O3 If* because of its strikingly strong emission lines (Walborn 1971). The extension of spectroscopy to the UV confirmed the extreme character of HD 93129A (Walborn & Nichols-Bohlin 1987). As already noted by Walborn (1971), Conti & Frost (1977), Moffat (1978) the spectrum of HD 93129A is very similar to Wolf-Rayet stars of spectral type WN6 or WN7. HD 93129A, obviously, has an extremely strong wind.

In our analysis, we investigate optical lines such as N III 4640 Å, N IV 4058 Å, N V 4605 Å, C III 4650 Å, C IV 4657 Å, 4657 Å together with lines in the UV (IUE) and FUV (ORFEUS) using an improved version of the hydrodynamic model atmosphere code described in Pauldrach et al. (PKPBH). Simultaneously, we also model the FUV absorption lines of the molecular and atomic interstellar spectrum. This analysis is presented in Sect. 3 after a short description of the observational data in Sect. 2. In Sect. 4 we discuss radiation driven wind models for HD 93129A and compare the computed terminal velocity and mass-loss rate with the observed values. In Sect. 5 we summarize the status of HD 93129A in the context of massive star evolution.

2. Observations and reduction

The FUV spectrum was observed with ORFEUS (Krämer et al. 1990, Krämer & Mandel 1993) and the Berkeley Spectrometer (Hurwitz & Bowyer 1991) in September 1993. The spectral range is 900 to 1170 Å and the resolution corresponds to 110 km/s. The integration time was 3045 seconds leading to a S/N of 10–30. The data reduction was carried out in Berkeley with a special package developed for this instrument.

The UV was observed with IUE (SWP 14007, see Howarth and Prinja, (1989)) in the spectral range from 1150 to 1800 A. The spectral resolution corresponds to 30 km/s and the S/N is approximately 30.

The optical spectra were taken with the EMMI spectrograph on the ESO NTT by D.J. Lennon in December 1992. Spectral ranges of 3930 to 4750Å and 6300 to 6800Å were covered with a resolution of approximately 1.0 Å and with a S/N of roughly 200.

3. The quantitative analysis

As is to be expected from the strong interstellar Lyman-α line in the IUE spectrum and the reddening (E(B-V)=0.54) towards HD 93129A (Simon et al., 1983), the FUV spectrum of HD 93129A is contaminated by a rich spectrum of interstellar absorption lines. Strong molecular absorption lines of H_2 (Lyman and Werner bands), H_2O, CO, and N_2 can be identified, as well as neutral species such as H, C, N, O, Ar and Cl plus many ionized species like C II, C III, ..., O VI, P II-P V, Fe II, Fe III.

To disentangle the blends of stellar and interstellar lines it is necessary to perform spectrum synthesis calculations for both systems. We begin with the interstellar lines in Sect. 3.1 and then describe the work on the stellar lines in the following sections.

3.1. Analysis of the interstellar FUV spectrum

The most dominant interstellar lines in the ORFEUS spectrum are those of the Lyman and Werner bands of H_2 from the ground electronic state $X\,^1\Sigma_g^+$ to the upper states $B\,^1\Sigma_u^+$ and $C\,^1\Pi_u^\pm$, respectively. These lines were the starting point for the synthesis of the molecular spectrum. We first concentrated on the spectral region between 1047 to 1055 Å which, according to the synthesis of the stellar spectrum, should be free of significant stellar lines (see Fig. 1). Apart from one single interstellar Ar I line, there are exclusively H_2 and HD lines of the groundstate of para- and ortho hydrogen present, as well as lines from higher excitation states. An identification list for the spectral synthesis is given in Table 1. The molecular and atomic data used for these calculations are from Morton & Dinerstein (1976), Morton (1975), (1991), Allison & Dalgarno (1970), Dabrowski & Herzberg (1974), (1975) and are completed according to Morton & Dinerstein (1976). The code we used to carry out the profile calculations is one originally due to Davenhall (1977) ported to STARLINK by A.P. Phillips. It is based on the physics described by Strömgren (1948) and yields wavelengths, oscillator strengths f, natural damping constant γ and statistical weights for each transition and velocity dispersions b, cloud velocities v and column densities n to describe the interstellar clouds.

The spectral resolution of the ORFEUS-1 data does not allow independent measurement of the velocities and contributions of individual clouds in the line of sight. Therefore, we have to rely on information obtained from other spectral domains. Walborn et al. (1984) found that the strongest contributions to

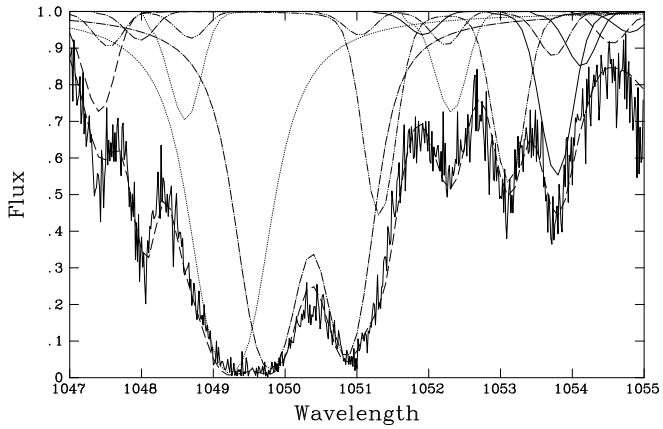

Fig. 1. The ORFEUS spectrum of HD 93129A between 1047 and 1055Å, which consists mostly of molecular lines of H_2 and HD. The dashed curve represents the final interstellar spectrum synthesis. The contribution of individual molecular lines are also shown, the strongest components belong to H_2 J=0 at 1049.4 Å and J=1 at 1050.0 and 1051.0 Å. For additional components, see Table 3.1

interstellar lines of neutral or low ionization stages towards the Carina nebula originate from clouds with velocities of -90 and -30 km/s. We assume that the molecular lines correspond to these clouds. For the velocity dispersion of molecular hydrogen we adopt 1.6 and 3.6 km/s, respectively, following Spitzer et al. (1973).

With these assumptions, the only free parameters are the column densities in the absorbing states. We start with the ground-state lines of para and ortho hydrogen, the strongest lines in the spectral interval shown in Fig. 1 (λ 1049.4 R(0), λ 1050.0 R(1) and λ 1051.0 P(1)) and derive column densities of 7.4×10^{19} particles per cm^3. The next step is to estimate column densities for those excited levels that dominate the observed absorption features (examples in Fig. 1 are listed in Table 1).

The procedure is then extended to other regions of the FUV spectrum, where additional isolated or weakly blended features of excited levels of H_2 or HD are found and column densities can be determined or checked for consistency. Finally, the whole procedure is iterated, since the additional levels give rise to additional weak line features in regions previously dominated by stronger transitions and modify the synthesized spectrum. Fig. 1 shows a typical example for the contribution of strong and weak components.

Table 2 contains all the H_2 and HD column densities that have been determined by this process. Note that some values are highly uncertain because no clearly unblended features could be found for them.

Similarly we derive column densities for the second most abundant molecule CO. Due to the weakness of the CO lines and the existing stellar and interstellar blends only the λ 1076.03 and 1087.87 lines are available for an analysis. These lines seem to be dominated by the groundstate components. Thus we calculate the R(0) transitions of $E\,^1\Pi - X\,^1\Sigma^+$ and $C\,^1\Sigma^+ - X\,^1\Sigma^+$ using atomic data from Morton & Noreau (1994) and derive a value of log N(CO) = 15.6 as an upper limit for the column density of CO.

Table 1. Interstellar lines between 1047 and 1055Å with molecular data used

Wave.	Ele.	Transition	f-value	gl	gu	γ
1047.6	H_2	B – X 5-0 P(4)	0.0105	9	21	1.37e+9
1047.7	H_2	B – X 6-0 R(7)	0.0141	45	17	1.30e+9
1048.1	HD	B – X 5-0 P(3)	0.0086	7	5	1.43e+9
1048.2	Ar I	$3p^6\ ^1S - 4s'[\frac{1}{2}]^o$	0.24	1	3	4.94e+8
1048.8	HD	B – X 6-0 P(6)	0.0104	13	11	1.34e+9
1048.8	H_2	B – X 5-0 R(5)	0.0139	33	13	1.37e+9
1048.9	HD	B – X 5-0 R(4)	0.0111	9	11	1.43e+9
1049.4	H_2	B – X 4-0 R(0)	0.0235	1	9	1.45e+9
1050.0	H_2	B – X 4-0 R(1)	0.0160	9	5	1.45e+9
1051.0	H_2	B – X 4-0 P(1)	0.0075	9	1	1.45e+9
1051.2	HD	B – X 5-0 P(4)	0.0088	9	7	1.43e+9
1051.5	H_2	B – X 4-0 R(2)	0.0147	5	21	1.45e+9
1052.1	HD	B – X 5-0 R(5)	0.0108	11	13	1.43e+9
1052.4	H_2	B – X 6-0 P(7)	0.0123	45	13	1.30e+9
1052.5	H_2	B – X 5-0 P(5)	0.0105	33	9	1.37e+9
1053.3	H_2	B – X 4-0 P(2)	0.0088	5	9	1.45e+9
1053.9	H_2	B – X 4-0 R(3)	0.0142	21	9	1.45e+9
1053.9	H_2	B – X 5-0 R(6)	0.0136	13	45	1.37e+9
1054.3	HD	B – X 4-0 R(0)	0.0161	1	3	1.50e+9
1054.7	HD	B – X 4-0 R(1)	0.0107	3	5	1.50e+9
1055.0	HD	B – X 5-0 P(5)	0.0090	11	9	1.43e+9

We have also determined column densities for the atomic and ionic species producing interstellar absorption lines in the ORFEUS-1 spectral range. Following Walborn et al. (1984) we have adopted velocity dispersions of 15 and 20 km/sec, respectively for these species. The resulting column densities are also given in Table 2.

The main purpose of our analysis of the interstellar lines is to disentangle their influence on the stellar spectrum and to avoid misinterpretation of the latter. On the other hand, it turns out that a careful spectrum synthesis of the stellar spectrum is equally important if one wishes to determine interstellar column densities. This is demonstrated in Fig. 2 – Fig. 4 for interstellar O VI, O I and P II. Our experiences lead us to conclude that a general reinvestigation of the FUV data obtained with Copernicus might be worthwhile.

A full identification of the stellar and interstellar spectrum is given in Table 3 – Table 5.

The data presented in Table 2 can also be used for the interpretation of the physical status of the Carina star forming cloud. This will be done in more detail in a separate paper. Here, we briefly discuss a few of the results.

The H_2 column densities allow a rough estimate of excitation temperatures. We obtain 77K from the ratio of ortho (J=1) to para hydrogen (J=0) and 105, 146, 230 K for the excitation of

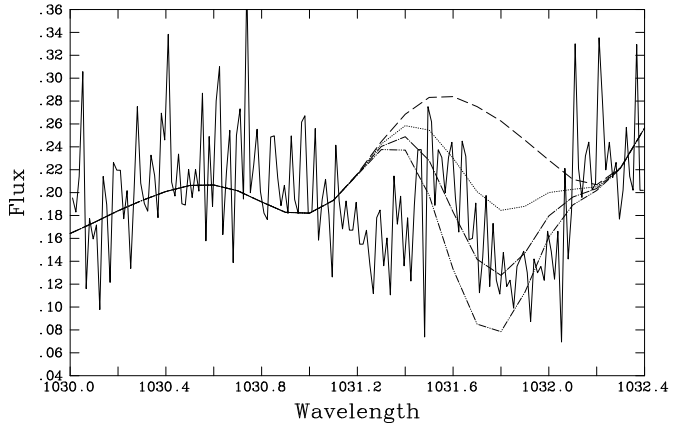

Fig. 2. The dashed curve corresponds to spectrum synthesis including the stellar wind O VI line and interstellar H_2. The three other curves include the additional contribution of interstellar O VI with log N(O VI)/cm^2= 14.1, 14.5 and 14.9. Note that the spectrum synthesis is incomplete around 1031.3Å

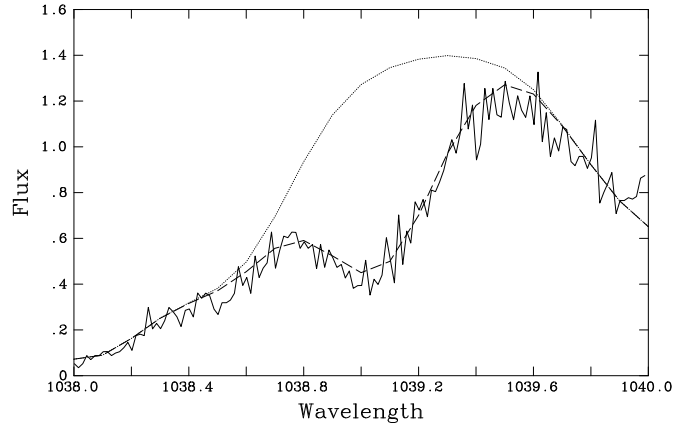

Fig. 3. The ORFEUS spectrum around interstellar O I. The dotted curve contains the contribution of stellar O VI and interstellar H_2, whereas the dashed curve also includes interstellar O I.

J=2, 3, 4 relative to J=0. This is in agreement with the results of Spitzer et al. (1973), (1974) and Spitzer & Cochran (1973) for the excitation of molecular hydrogen towards less distant hot stars in clouds of lower extinction and the discussion of NLTE effects on H_2 level populations (Dalgarno et al., (1973), Spitzer & Zweibel (1974), Jura (1975a), (1975b)). On the other hand, the fraction $f = 2\,N(\mathrm{H_2})/(N(H\,\mathrm{I}) + 2\,N(\mathrm{H_2})) = 0.1$ of hydrogen atoms in the molecular stage is smaller than found by Spitzer et al. This might be caused by dissociation due to the enormous UV radiation field of HD 93129A. The value of 10^{-5} for the ratio of HD over H_2 (for J=0 and J=1) is larger than found by Spitzer et al. and requires a more detailed discussion in terms of UV shielding and molecule formation.

If CO and H_2 are present in the same clouds, the upper limit for the ratio N(CO)/N(H_2) is 2.6×10^{-5} which is similar to the value of 1.3×10^{-5} found by Morton (1975) for ζ Ophiuchi.

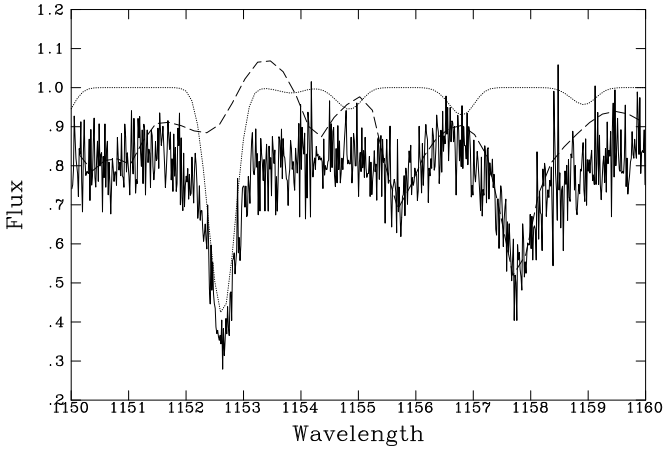

Fig. 4. The ORFEUS spectrum around interstellar lines of P II. The interstellar P II contribution is given by the dotted curve, whereas the dashed curve represents the total contribution of all stellar and interstellar lines.

Table 2. Derived column densities of interstellar atomic and molecular states. The value for P I is from the IUE spectrum. Values giving only upper limits are marked by a colon.

Level	log N	Level	log N	Level	log N
H_2 (J=0)	19.9	N II J=0	16.4	P V J=$\frac{1}{2}$	13.6:
H_2 (J=1)	19.9	N II J=1	14.8	S III J=0	15.1
H_2 (J=2)	18.5	N II J=2	14.8	S III J=1	14.8:
H_2 (J=3)	18.2	N III J=$\frac{1}{2}$	14.8	S III J=2	14.8:
H_2 (J=4)	17.7	O I J=2	16.4	S IV J=$\frac{1}{2}$	14.8:
H_2 (J=5)	17.7	O I J=1	14.7	Cl I J=1$\frac{1}{2}$	14.4
HD (J=0)	15.1	O VI J=$\frac{1}{2}$	14.6	Cl I J=$\frac{1}{2}$	14.0:
HD (J=1)	15.1	Si II J=$\frac{1}{2}$	14.6	Cl II J=2	14.6
H I J=$\frac{1}{2}$	21.4	Si II J=1$\frac{1}{2}$	15.5	Cl II J=1	14.3:
C I J=0	14.9	P I J=1$\frac{1}{2}$	12.9:	Ar I J=0	14.3
C I J=1	14.5	P II J=0	14.5	Fe II J=4$\frac{1}{2}$	14.9
C I J=2	14.1	P II J=1	13.7	Fe II J=3$\frac{1}{2}$	13.9
C II J=$\frac{1}{2}$	15.5	P II J=2	13.6	Fe II J=2$\frac{1}{2}$	13.8
C II J=1$\frac{1}{2}$	15.4	P III J=$\frac{1}{2}$	14.1	Fe II J=1$\frac{1}{2}$	13.3:
C III J=0	17.1	P III J=1$\frac{1}{2}$	14.0:	Fe II J=$\frac{1}{2}$	13.3:
N I J=1$\frac{1}{2}$	15.6	P IV J=0	13.8	FeIII J=4	13.7

The abundance pattern of ions in ionization stages I and II relative to neutral hydrogen shows depletion for N, P, Si, and Fe, as observed for other lines of sight, whereas the depletion for C, O and Ar appears to be larger than normal (Jenkins et al. 1983, York et al. 1983, Shull & York 1977, Spitzer 1975, Morton & Hu 1975). From the weak lines of Cl I and Cl II we conclude that chlorine is almost undepleted, which is in agreement with Jura & York (1978) and their analysis of Copernicus spectra of ten nearby objects.

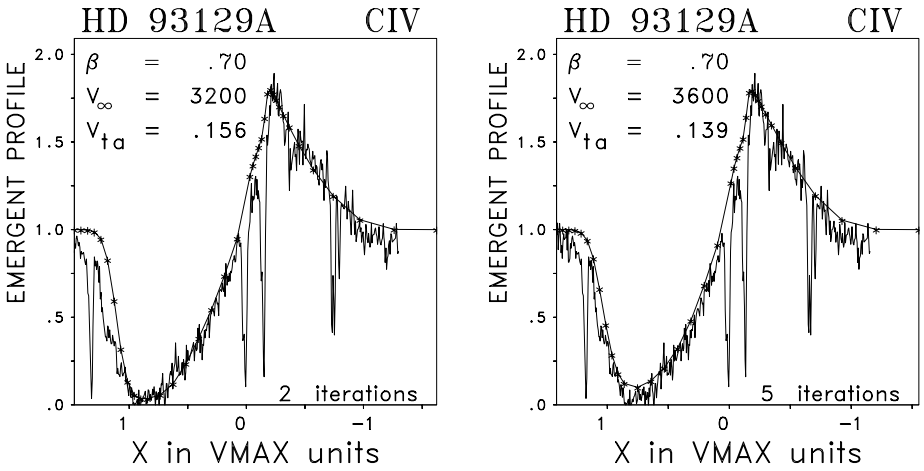

Fig. 5. Line fits to the P-Cygni profile of C IV with V_∞=3200 km s^{-1} and V_∞=3600 km s^{-1}. X is the Doppler shift relative to the laboratory wavelength of the blue doublet component in units of the terminal velocity V_∞. $V_{\rm ta}$ is the microturbulence velocity in units of V_∞.

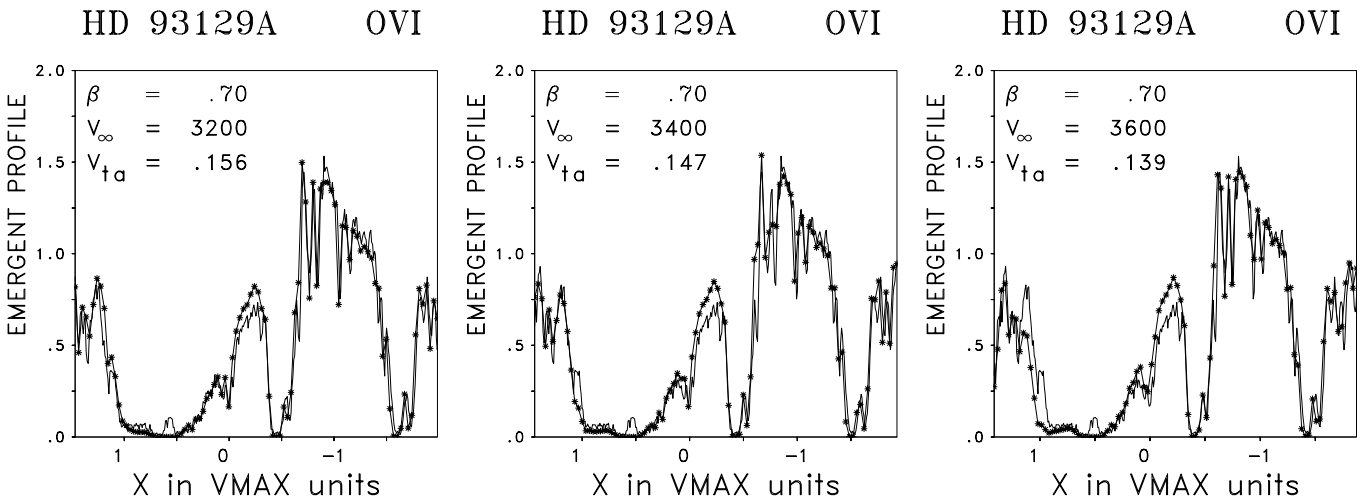

Fig. 6. Line fits to the P-Cygni profiles of O VI with V_∞=3200 km s^{-1}, V_∞=3400 km s^{-1}, and V_∞=3600 km s^{-1}. The fits of the blue wing become increasingly worse with increasing V_∞. Note, that the lower part of the blue edge is not affected by blends of interstellar lines.

3.2. The terminal velocity of the stellar wind

The terminal velocity of the stellar wind can be determined from the P Cygni profiles of stronger resonance lines by comparing with NLTE radiative transfer calculations in spherically expanding atmospheres. We use the method developed by Haser (1995), which is briefly described by Haser et al. (1995). This method is an extension of the work of Hamann (1981), Lamers et al. (1987) and Groenewegen & Lamers (1989). The line fits yield V_∞ together with microturbulence parameter $V_{\rm turb}$ (given in units of V_∞) which is the broadening parameter for the local atomic absorption coefficient in the stellar wind. Note that the most likely interpretation of $V_{\rm turb}$ is that it simulates the effects of the presence non-monotonic velocity fields with multiple shocks (Lucy 1982, 1983, Puls et al. 1993) superimposed to the smooth stellar wind flow. Thus, $V_{\rm turb}$ may be taken as a measure of the shock jump velocities occuring in stellar wind instabilities (see Pauldrach et al., 1994b). In the radiative transfer calculation it affects mostly the steepness of the blue absorption edge and the position of the emission peak in the P Cygni profile, whereas V_∞ influences the blueshift of the absorption edge.

Using the IUE spectrum only results in a rather uncertain determination of V_∞ between 3200 to 3600 km/s. The reasons are: (i) only the C IVλ1550 resonance line can be used for a fit. N Vλ1240 is far too noisy and its absorption trough overlaps with the strong interstellar Lyman-α absorption profile such that the blue wing cannot be reconstructed with a Lyman-α fit. (ii) The blue wing of the C IV profile is unusually shallow, demanding very high values for the microturbulence parameter ($V_{\rm ta}$) larger than $0.12\,V_\infty$. Different combinations of V_∞ and $V_{\rm ta}$ yield similarly good fits for $V_\infty = 3200 \ldots 3600$ km s^{-1} (see Fig. 5) resulting in nearly indistinguishable model profiles.

This situation is much improved using the O VI profile from the ORFEUS-1 observation. Here the best line fit results in an accurate value for the terminal velocity of V_∞ = 3200 km s^{-1} (see Fig. 6). Different combinations of the microturbulence and the terminal velocity might still allow a slightly larger V_∞ = 3400 km s^{-1}, but this should be regarded as the upper limit. The remaining uncertainty of $\lesssim$ 200 km s^{-1} lies within the range of the so called blue edge variability of saturated P-Cygni profiles (see Henrichs 1991) and thus cannot be improved any further. From the above we regard V_∞ = 3200 km s^{-1} as the best value for the terminal wind velocity of HD 93129 A. Together with the redetermination of the mass-loss rate in Sect. 3.6 this will be used to discuss the mechanical momentum and energy of the wind of this extremely luminous star.

The best fit for the microturbulence parameter yields $V_{\rm ta}$=1.56 corresponding to a turbulent velocity of 500 km/s, a very high value. This will be of importance for Sect. 3.8, in which we investigate the shock emission in the wind of HD 93129A.

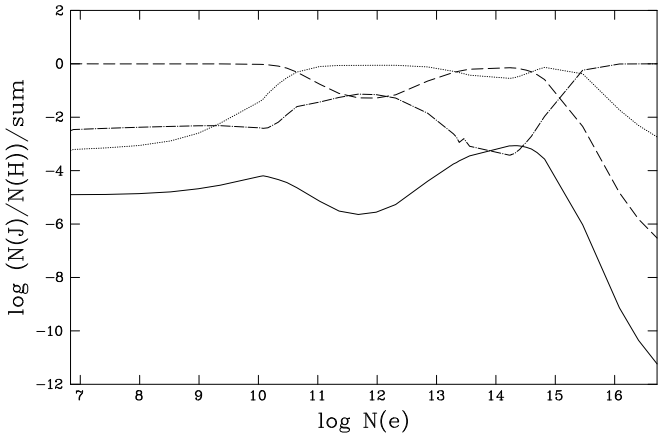

Fig. 7. Ionization fractions of N III (solid), N IV (dashed), N V (dotted) and N VI (dashed-dotted) as a function of atmospheric electron density for $T_{\rm eff}$=50000K. The optical nitrogen lines are formed between log N(e)=10.7 and log N(e)=14.

3.3. The model atmosphere code

Since the strong stellar wind outflow of HD 93129A is affecting almost all lines in the optical to FUV stellar spectrum, a hydro dynamical model atmosphere code is needed for the spectrum synthesis. We use the atmospheric NLTE code for radiation driven winds described in detail by PKPBH. A few significant improvements have been implemented in the code since this publication appeared. They are discussed in the following.

In principle line blocking in NLTE for all 10^6 lines can now be included in the calculation of the local radiation field for solving the rate equations (Sellmaier et al., 1996, Sellmaier, 1996). However, in order to save a significant amount of computer time, we have a second option which introduces a frequentially and spatially smoothed quasi-continuum background opacity so that the emergent flux is similar to the version with exact line opacities. This version has been used throughout the paper to calculate the local incident radiation field at every depth in the wind, which is needed to solve the rate equations for the occupation numbers.

To also account for weaker lines formed close to the region of continuum formation we abandon the pure Sobolev approximation and use the Sobolev approximation with continuum instead for the calculation of radiative bound-bound transition probabilities (Hummer & Rybicki 1985, Puls & Hummer 1988, Puls 1991). These are given by

$$R_{ij} \;=\; B_{ij}\left(\overline{\beta_C\, I_C} + \overline{U}\, S_C\right) \qquad (1)$$

$$R_{ji} \;=\; B_{ji}\left(\overline{\beta_C\, I_C} + \overline{U}\, S_C\right) + A_{ji}\left(\beta + \overline{U}\right) \qquad (2)$$

(Puls 1991) A_{ji}, B_{ji} and B_{ij} being the Einstein coefficients, β the usual escape probability, derived from the Sobolev optical depth τ_S. The additional quantities are $S_{\rm C}$, the continuum source function, $\overline{U}$ = $1/4\pi \int d\omega U\left(\tau_S, k'_C/k'_L\right)$ ($k'_L = k_L/\delta\,\nu_D$) the interaction function, introduced by Hummer & Rybicki (1985) and $\overline{\beta_C\, I_C}$ the generalized intensity of radiation in the line frequencies, incident on the line formation region, derived from the solution of the continuum transfer equation.

A very exact and fast approximation for the calculation of $\overline{\beta_C\, I_C}$ is given in Appendix A, where we also treat the case of level inversions and negative Sobolev optical depths.

A crucial ingredient of the stellar wind NLTE calculations by PKPBH is the EUV and soft X-ray emission by stellar wind shocks affecting the observable high ionization stages in the FUV. In our analysis of HD 93129A we adopt essentially the same procedure to take shock emission into account. However, as an improvement we use the full cooling function including correctly line emission (Cox and Raymond, (1985), Raymond and Smith, (1987), Raymond, (1988)) to calculate the shock emission coefficient instead of taking into account the free-free emission multiplied by a wavelenght independent factor, as it was done by PKPBH.

Further improvements concern the line list and the atomic models used for the solution of the rate equations. Here the status is that described in Sellmaier et al. (1996), except that in addition a more detailed atomic model for phosphorus is introduced (see Appendix B) to match the corresponding lines in the ORFEUS-1 spectral range.

3.4. An independent determination of $T_{\rm eff}$ using the nitrogen ionization equilibrium

The standard technique for the determination of the effective temperature of O-stars is the use of the helium ionization equilibrium (Kudritzki & Hummer 1990, and references therein). However, as found by Herrero et al. (1992) in their systematic study of O-stars, this temperature indicator can lead to uncertainties depending on which of the He I lines are used (see also Herrero 1994). Since for the hottest O-stars of spectral type O3 only one very weak HeI line (HeI 4471) is marginally detectable (Kudritzki 1980, Simon et al. 1983, Kudritzki 1992), it

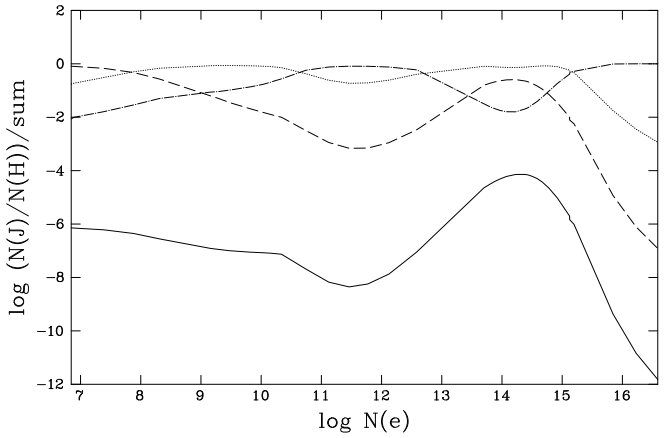

Fig. 8. Same as Fig. 7 but for $T_{\rm eff}$=53000K

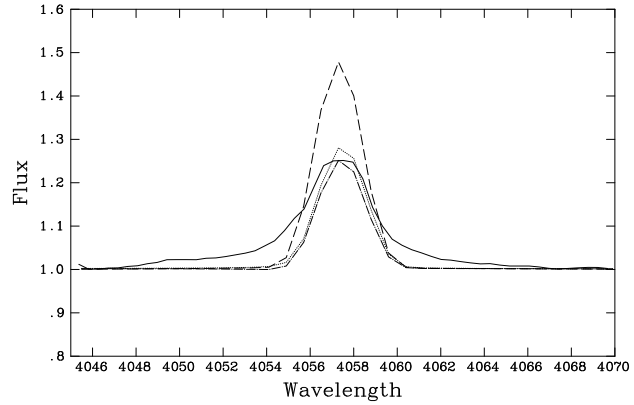

Fig. 9. N IV 4059 Å (**solid**) compared with theoretical profiles for models assuming temperatures of 50000 K (dashed), 52000 K (dotted), 53000 K (dashed-dotted).

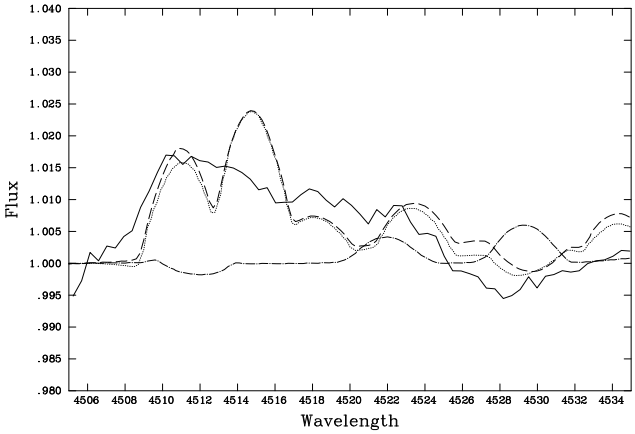

Fig. 10. N III 4519 Å quartet lines between 4511 and 4534 Å (**solid**) compared with theoretical profiles for models assuming temperatures of 50000 K (dashed), 52000 K (dotted), 53000 K (dashed-dotted).

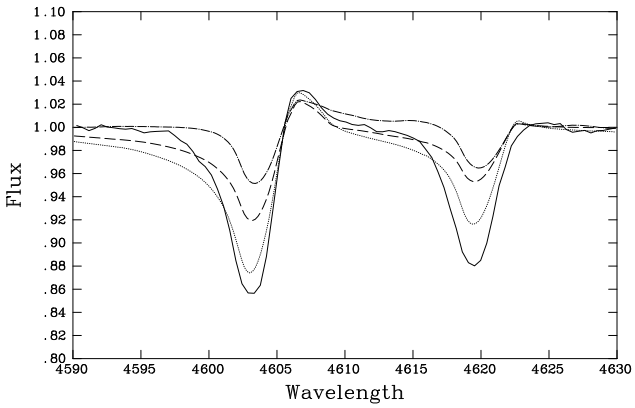

Fig. 11. N V 4605 Å doublet (**solid**) compared with theoretical profiles for models assuming temperatures of 50000 K (dashed), 52000 K (dotted), 53000 K (dashed-dotted).

is important to look for new independent methods to determine $T_{\rm eff}$.

In principle, the ionization equilibrium of nitrogen appears to be ideal for this purpose, since excited lines of N III, N IV and N V can be easily identified in the spectra of O3-stars. However, as is well known from the pioneering work of Mihalas & Hummer (1973), the nitrogen lines are severely affected by the stellar wind velocity fields and show emission when the winds are strong. As a consequence, up to now no attempt has been made to use these lines for a determination of $T_{\rm eff}$ in O3-stars. This is very unfortunate, since in particular HD 93129A shows weak emission of N III, strong emission of N IV and pronounced N V P-Cygni profiles (for line identifications used in the spectrum synthesis of our optical spectra see Table 6) so that it should be possible to find additional constraints on $T_{\rm eff}$.

Therefore, we investigate whether our hydrodynamic model atmosphere code allows us to obtain an independent value for $T_{\rm eff}$. For this purpose we have calculated a small grid of three models with $T_{\rm eff}$= 50000, 52000 and 53000 K, respectively (models 1 to 3 in Table 7) for which we keep the gravity fixed at the value determined by Puls et al. (1996) from the fit of the Hγ profile. The terminal velocity V_∞ is also kept fixed to the observed value. Since the value of the mass-loss rate $\dot{M}$ determined from the fit of the Hα emission profile (see Sect. 3.6) depends weakly on the adopted $T_{\rm eff}$ (see Puls et al. 1996, for details), $\dot{M}$ is varied slightly to be consistent with Hα. The same is done with the stellar radius which follows from the distance and the apparent de$-$reddened magnitude, once $T_{\rm eff}$ is specified. The nitrogen abundance is adopted to be two times solar (see Sect. 3.7) and also kept constant. (All other parameters in Table 7 will be introduced later in the text).

Fig. 9 and 11 show the profiles of the N IV 4058 Å emission and the N V 4605 Å wind lines compared with the calculations. The N V lines show maximum strength at $T_{\rm eff}$=52000 K. The reason for this is that from 50000 K to 52000 K the excitation of the 3s levels of N V is enhanced in the line forming region around the sonic point but that for higher temperatures the ionization to N VI becomes the dominant effect. The N IV emission decreases from 50000 K to 52000 K and then remains constant. This is caused by a decrease in the population of the N IV 3p level due to enhanced ionization to N V which is then partially

Table 7. Parameters of calculated models

No.	$T_{\rm eff}$ [K]	$log g$	R_* [Rsun]	$\dot{M}$ [(-6) $M_\odot$ /yr]	V_∞ [km/s]	v_t [V_∞]	$log\, L_{\rm x}$	Y_{CNO}
1	50000	3.95	20.0	17.7	3200	.16	32.2	0.2 2.0 0.3
2	52000	3.95	19.7	18.0	3200	.16	32.2	0.2 2.0 0.3
3	53000	3.95	19.5	16.0	3200	.16	32.2	0.2 2.0 0.3
4	52000	3.95	19.7	18.0	3200	.16	32.2	1.0 1.0 1.0
5	52000	3.95	19.7	18.0	3200	.16	32.2	0.1 4.0 0.2
6	52000	3.95	19.7	18.0	3200	.16	33.7	0.2 2.0 0.3
7	52000	3.95	19.7	18.0	3200	.16	31.5	0.2 2.0 0.3

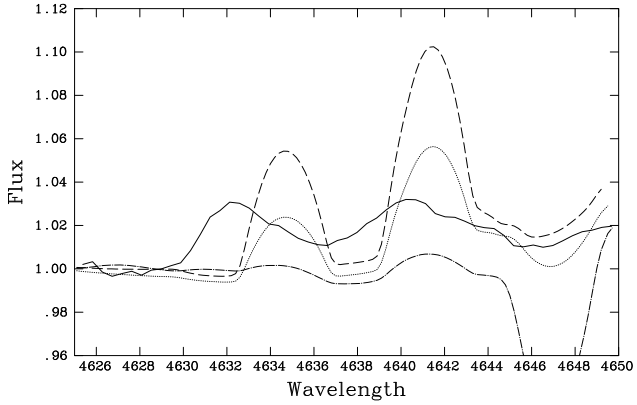

Fig. 12. N III 4640 Å doublet (**solid**) compared with theoretical profiles for models assuming temperatures of 50000 K (dashed), 52000 K (dotted), 53000 K (dashed-dotted). Note that Si IV 4631 is not reproduced properly by the spectrum synthesis.

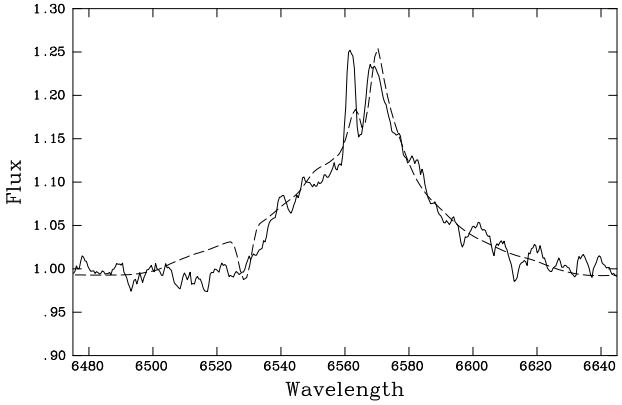

Fig. 13. Observed Hα profile (**solid**) compared with the calculation assuming a mass loss of 18×10^{-6} $M_\odot$/yr (dashed). Note that the blue narrow emission peak originates from the H II-region emission.

compensated by enhanced excitation. (Fig. 7 and 8 give the nitrogen ionization stratifications for the models with different $T_{\rm eff}$).

We conclude from Figs. 9 and 11 that $T_{\rm eff}$=52000 $\pm$ 1000 K is a reasonable estimate for HD 93129A. This is not too different from the 50500 $\pm$ 1500 K found by Kudritzki & Hummer (1990) using the helium ionization equilibrium.

The weak N III emission lines can be used as a consistency check with regard to $T_{\rm eff}$. This is done in Fig. 10 and 12. Bearing in mind that our continuum rectification is uncertain by 1%, we regard this as a confirmation of the result obtained from N IV and N V.

The quality of the fits in Fig. 9 and 11 requires a few comments. The calculations for N IV fail to reproduce the far wings of the emission line. This is caused by the fact that above the layer where the intrinsically rather narrow emission line is formed there is still an electron layer of sufficient optical depth (because of the high rate of mass-loss) to produce the wide wings by incoherent scattering. Incoherent electron scattering has not been included in the calculation so far.

The N V calculations produce blue wings that are slightly too strong. This could be corrected with a somewhat steeper velocity field above the sonic point up to 900 km/s or by marginally decreasing the ionization or excitation in the same layers of the expanding wind.

In general, we stress however that the use of the hydrodynamic model atmosphere code has made it possible for the first time to use the ionization equilibrium of the optical nitrogen lines for an independent determination of the effective temperature of an O3-star.

3.5. The argon ionization structure - a possible temperature indicator in the FUV

In the ORFEUS spectrum of HD 93129A we identify forbidden lines from the ground state of Ar VI and lines from the excited 3p ^{1}P$^{\rm o}$ level of Ar VII (see Table 3). Although they are severely blended with H_2, they might serve as additional temperature indicators, as can be seen from Figs. 17 and 18, which demonstrate the change of the argon ionization structure around the sonic point when $T_{\rm eff}$ is increased from 50000 K to 52000 K.

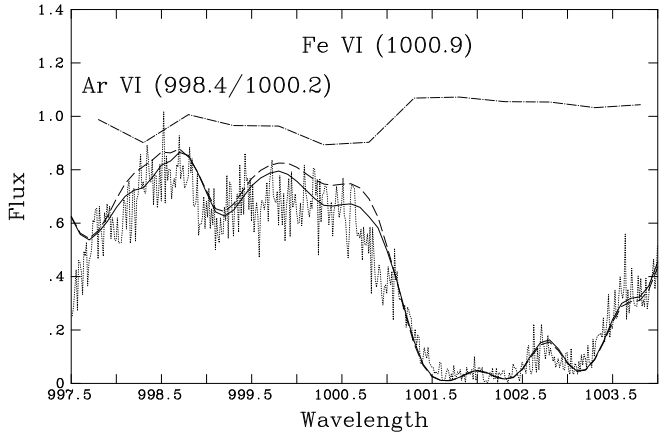

Fig. 14. The ORFEUS spectrum around the Ar VI ground state forbidden lines (dotted) compared with the stellar spectrum synthesis of our final model (dashed), the interstellar spectrum synthesis (dash-dotted) and a combination of the latter (solid).

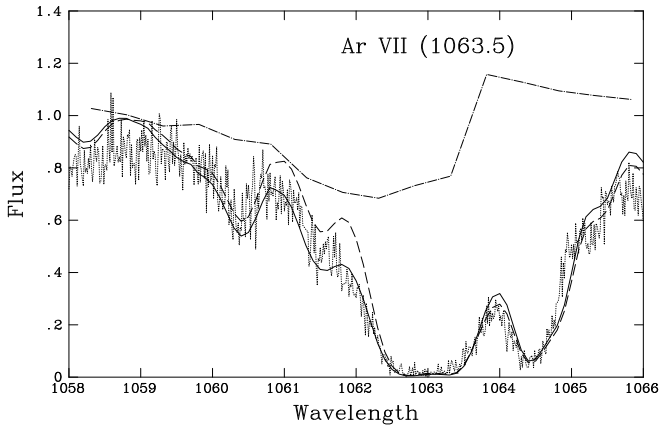

Fig. 15. Same as Fig. 14, but for Ar VII line.

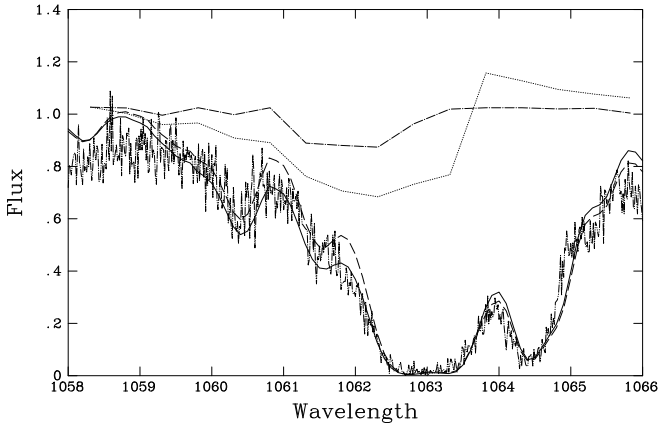

Fig. 16. The ORFEUS spectrum around Ar VII line (dash-dot-dotted) is compared with the stellar spectrum synthesis of our final model (dotted), model 1 assuming an effective temperature of 50000K (dashed-dotted) and the combination of both with the interstellar spectrum synthesis (solid and dashed, respectively).

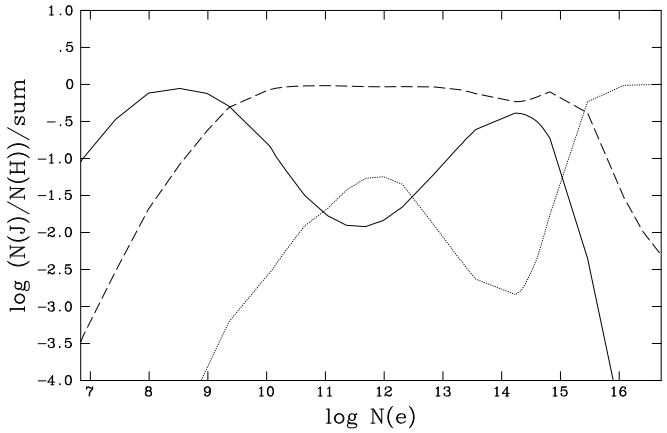

Fig. 17. Ionization fraction of Ar V (solid), Ar VI (dashed) and Ar VII (dotted) as a function of atmospheric electron density for $T_{\rm eff}$=50000K.

While the change in Ar VI is moderate, it is significant in Ar VII and we therefore expect the Ar VII line to exhibit a clear dependence on $T_{\rm eff}$. This is indeed the case, as is demonstrated in Figs. 14 and 15, although the strong blend with H_2 does not really allow a direct determination of $T_{\rm eff}$. However, for hot stars less affected by molecular hydrogen this line might prove to be extremely useful.

The Ar VI lines barely depend on $T_{\rm eff}$ since Ar VI remains the dominating ionization stage. However, one can use the weak features on top of the interstellar spectrum to conclude that the assumption of solar argon abundance must be roughly correct.

3.6. The rate of mass-loss

Puls et al.(1996) have recently published a new, very fast and rather accurate technique to determine mass-loss rates from Hα profiles by means of approximate NLTE radiative transfer calculations. They have applied this technique for a large sample of O-stars in the Galaxy, the LMC and the SMC. For HD 93129A they obtained a value of $22\times10^{-6}\,M_\odot$/yr, assuming an effective temperature of 50500K. It is interesting to check this using the result obtained with our hydrodynamic model atmosphere.

Fig. 13 shows the best fit of Hα that we could obtain. The corresponding mass-loss rate is $18\times10^{-6}\,M_\odot$/yr indicating that the approximate technique by Puls et al. is indeed sufficiently accurate.

3.7. CNO abundances from optical lines

In Sect. 3.4 we used a nitrogen abundance increased by a factor of two relative to the solar value. That this abundance is reasonable is demonstrated by Figs. 19 and 20 for N IV and N V, respectively.

In addition, we can use the C III/C IV emission/absorption complex in the blue wing of He II 4685.7Å to obtain a first estimate for the carbon abundance (Fig. 21). From the observed absence of stronger absorption dips we conclude that carbon

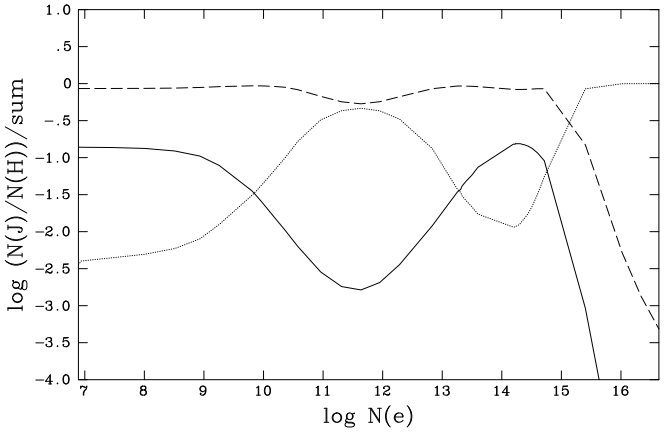

Fig. 18. Same as Fig. 17 but for $T_{\rm eff}$=52000K

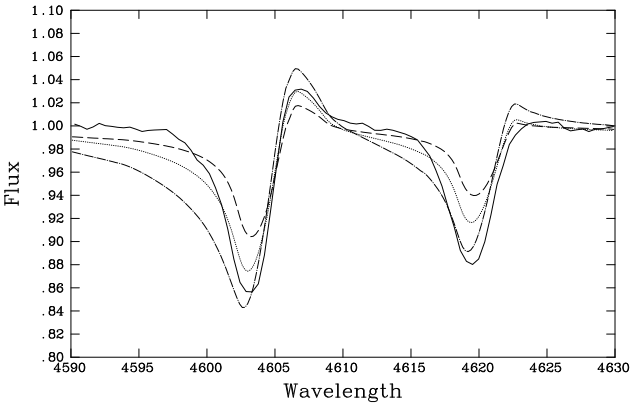

Fig. 20. Same as Fig. 19, but for the N V 4605 Å doublet.

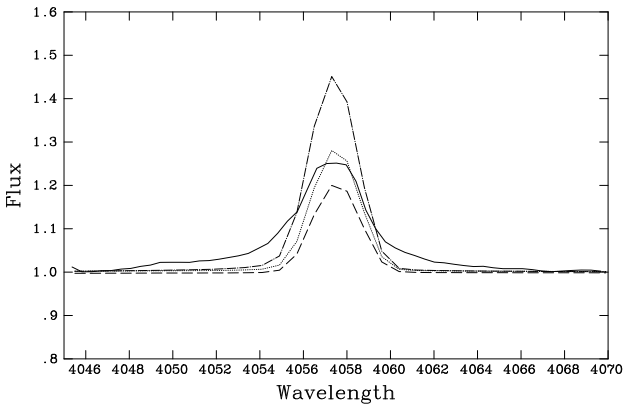

Fig. 19. N IV 4058 Å line of HD 93129A (solid) compared with theoretical profiles with an assumed solar nitrogen abundance (dashed), nitrogen overabundance of a factor 2 (dotted) and 4 (dashed-dotted). $T_{\rm eff}$=52000K is adopted.

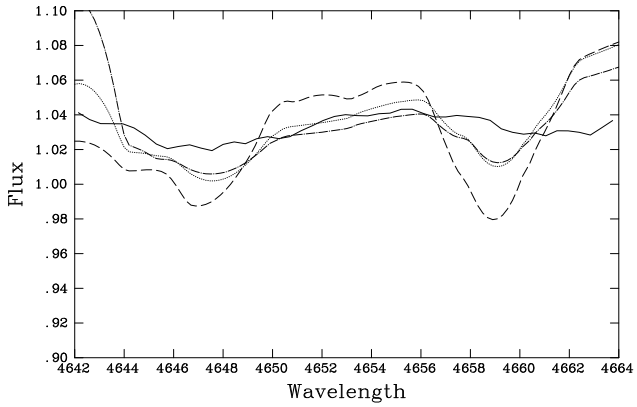

Fig. 21. C III, C IV complex (solid), in the blue wing of He II 4685.7Å compared with theoretical profiles for solar carbon abundance (dashed) and a carbon under abundance of a factor 0.2 (dotted) and 0.1 (dashed-dotted).

must be less abundant than solar. We adopt 0.2 solar but admit a large uncertainty for this value.

For oxygen we obtain a similar result from the O V lines at 4120 Å. The absence of observed absorption features leads to the conclusion that oxygen is reduced by 0.2 relative to the solar value (Fig. 22).

3.8. The FUV high ionization stages and shock emission

The effects of stellar wind shock emission on the ionization have been discussed in detail by PKPBH and Pauldrach et al. (1994b) for the case of ζ Puppis. It has been shown that the microturbulence velocity obtained from the fit of the UV resonance P-Cygni profiles agrees well with the shock jump velocity obtained by Hillier et al. (1993) from an analysis of the ROSAT PSPC spectrum by means of X-ray radiative transfer through a cold wind over which shocks of two different temperatures are randomly distributed. Both components contribute equally to the total X-ray luminosity, but the component with the lower shock temperature that dominates the very soft part of the X-ray spectrum is the one responsible for the production of very high ionization stages.

In the case of HD 93129A the soft X-ray component cannot be observed directly with ROSAT because of intrinsic absorption in the dense wind and additional interstellar absorption caused by the large interstellar column density (see Sect. 3.1). Only a harder component can be detected with a shock temperature of 1.1×10^7 K and a X-ray luminosity of $10^{33.8}$ erg/s (Kudritzki et al. 1996). Therefore, the only diagnostic tool to investigate whether shocks of lower temperature corresponding to the microturbulence velocity of 500 km/s (see Sect. 3.2) are present are the FUV high ionization features such as O VI.

We proceed in the same way as PKPBH (but see Sect. 3.3) and relate the shock jump velocity u to the velocity of the stellar wind (see Eq. 2 in PKPBH)

$$\frac{u(r)}{u_\infty} = \left(\frac{v(r)}{v_\infty}\right)^\gamma . \quad (3)$$

We choose γ=1 (changing γ between 0.5 to 1.5 had no influence on the results, as our test calculations showed). Then, we adjust the shock volume filling factor f so that a prespecified X-ray luminosity is produced (see PKPBH).

We start with $L_{\rm xsoft}$=33.8. This would be comparable to the case of ζ Puppis, where the low temperature shocks produce as

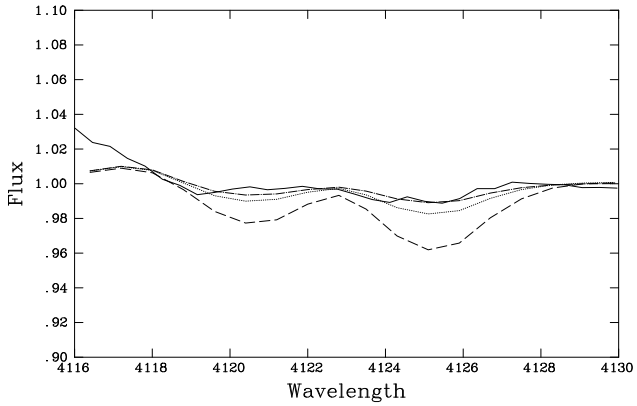

Fig. 22. O V lines at 4119, 4124 and 4126 Å (solid) compared with theoretical profiles for solar oxygen abundance (solid), oxygen under abundance of a factor 0.3 (dotted) and 0.2 (dashed-dotted).

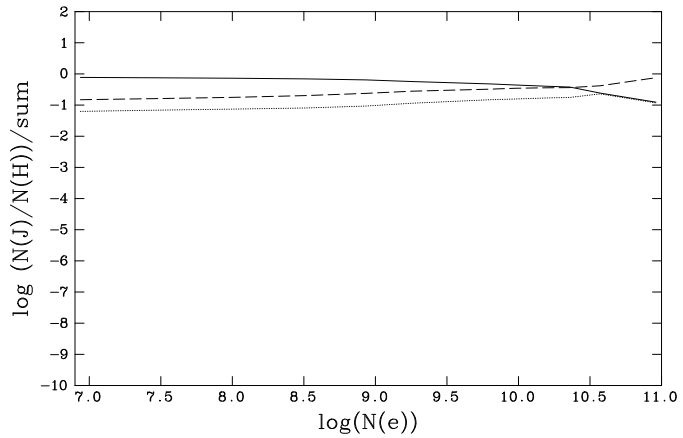

Fig. 23. Ionization fractions of O IV (solid), O V (dashed), O VI (dotted) as a function of electron density in the stellar wind for $log\ L_{xsoft}$=33.8.

much X-ray luminosity as the high temperature shocks. However, the calculated wind profile indicates that too much O VI is produced by ionization from O IV via O V to O VI (Fig. 23), which means that the fraction of low temperature shocks producing soft X-rays and EUV radiation must be smaller. On the other hand, if we reduce the shock emission to zero, the O VI line is much too weak (Fig. 27). The best fit is obtained for log L_{xsoft}=32.2 (Fig. 28). Figs. 23, 24 and 25 show the influence of the strength of the shock radiation field on the ionization fractions of oxygen.

The fact that the emission of soft X-rays is much smaller than the harder X-ray flux in the spectral range observable with ROSAT is very surprising and favours a model of two components of shocks rather than a model where the soft X-ray emission originates from the cooling zones of the shocks only (Feldmeier et al. 1996). It will be extremely important to extend this kind of study to other O-stars observed with ROSAT.

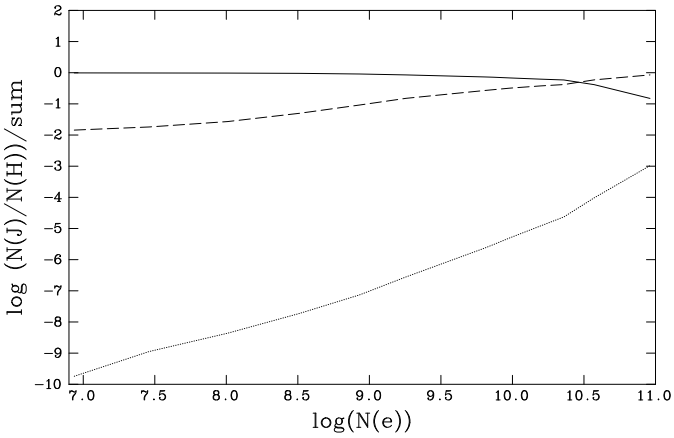

Fig. 24. Same as Fig. 23 but for log L_{xsoft}=0.

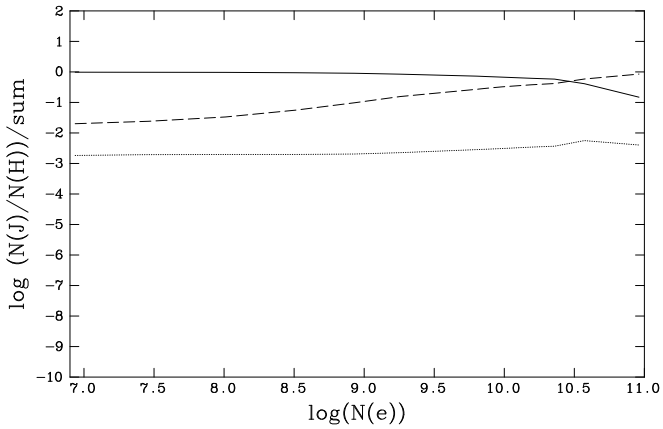

Fig. 25. Same as Fig. 23 but for log L_{xsoft}=32.2

3.9. Iron and nickel abundance

Both the FUV and UV spectra of HD 93129A contain many lines of iron group elements in high ionization stages which can be used for abundance estimates. As an example, we show the result of our spectrum synthesis in the region from 1130 to 1165 Å carried out for solar abundance (Figs. 29 and 30). We conclude that solar abundance is a good guess for iron and nickel.

3.10. Complete FUV and UV spectrum synthesis

Figs. 31 and 32 show the full ORFEUS and IUE spectra of HD 93129A compared with the complete spectrum synthesis.

A few comments concerning apparent discrepancies are necessary. The first one concerns P V, for which a solar abundance was assumed. Both P V resonance doublet components are wind lines that extend blue ward down to 1105 Å. We attribute the remaining discrepancies to CO and H_2O molecular lines missing in the interstellar spectrum synthesis and conclude that solar abundance is a good assumption.

Another obvious discrepancy is found redward of N V between 1240 to 1260 Å in the IUE spectrum. Here our code

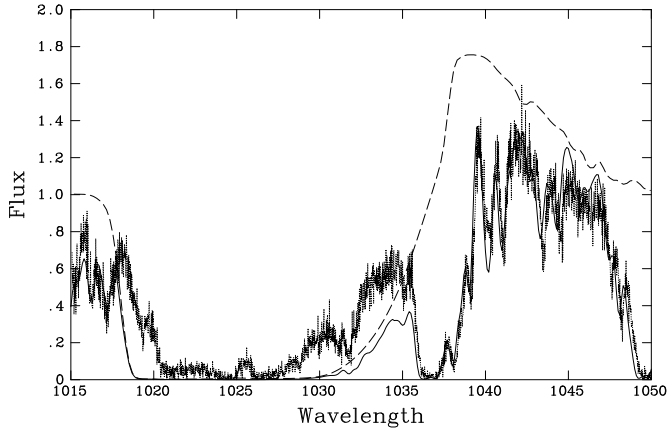

Fig. 26. O VI line profile compared with the purely stellar spectrum synthesis (dashed) and the combined stellar and interstellar spectrum synthesis (solid). $log\ L_{\rm xsoft}$=33.8 was assumed

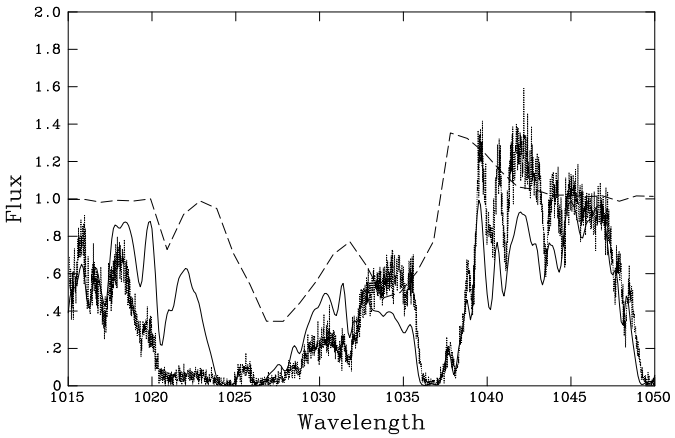

Fig. 27. Same as Fig. 26 but for $L_{\rm xsoft}$=0.

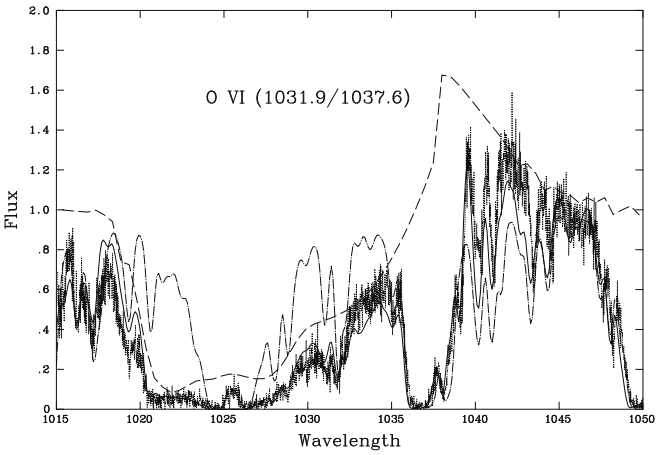

Fig. 28. Same as Fig. 26 but for $L_{\rm xsoft}$=32.2

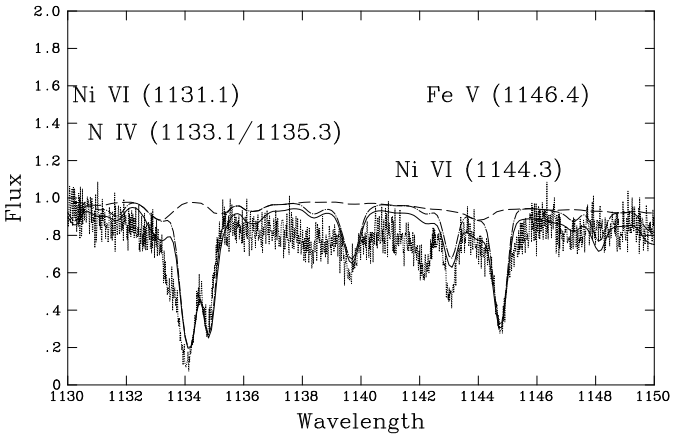

Fig. 29. The ORFEUS spectrum from 1130 to 1150 Å. The dashed curve gives the stellar spectrum synthesis, the solid curve also includes the interstellar lines.

produces Fe VI lines that are too strong in the outest part of the wind. At the moment, we have no explanation for this discrepancy. On the other hand, the Fe V and Fe VI lines between 1380 to 1480 and at 1599, 1616, 1655 and 1676 Å are in good agreement and confirm our assumption of solar abundance. The same is true for the Si IV resonance lines.

The wind lines of C IV, O V and N IV are reasonable well reproduced, although the fits are not yet perfect. Nevertheless, we regard this as a confirmation of the abundances adopted in Sect. 3.7.

The fit of He II 1640 reproduces the P-Cygni character of the line very well. Note that the absorption dip around 1626 Å is also due to the He II 1640 transition and is caused by helium recombining from He III to He II far out in the wind.

The impression of much better agreement in the ORFEUS spectrum is mostly due to the dominance of interstellar lines in the region.

In summary, the agreement between theory and observation is satisfying at this stage and is sufficient motivation for applications on additional objects in the future.

4. A consistent radiation driven wind model for HD 93129A

For the spectrum synthesis calculations presented so far the force multiplier parameters (see PKPBH and references therein) have been adjusted ad hoc to reproduce the empirically determined stellar wind parameters V_∞ and $\dot{M}$. However, we have also the option of solving the hydrodynamic equations of line driven winds consistently. In this case, effective temperature, gravity and radius together with the abundances are the input parameters and mass-loss rate and terminal velocity are obtained as the consistent result of radiation driven wind hydrodynamics. For HD 93129A with its very strong wind and its well determined stellar parameters this is a crucial test of the theory.

Carrying out the calculation we obtain

$V_{\infty \rm calc}$ = 3110 km/s

$\dot{M}_{\rm calc}$ = 20.8×10^{-6} $M_\odot$/yr

in excellent agreement with the observed values of 3200 km/s and 18×10$^{-6}M_\odot$/yr. The force multipliers are (see PKPBH) k=0.141, α=0.62 and δ=0.06. We conclude that the strong wind of HD 93129A is radiation driven and that the theory

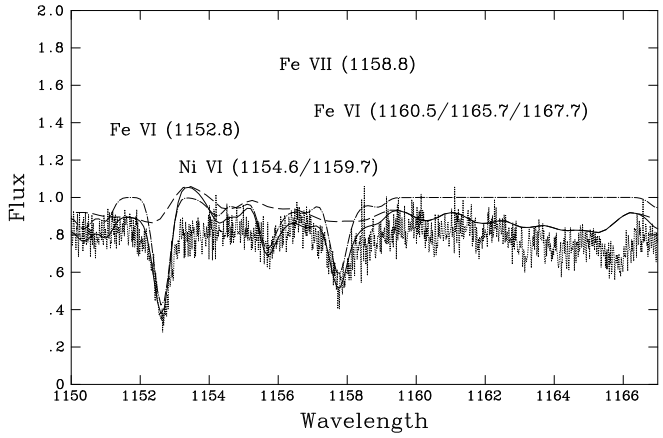

Fig. 30. Same as Fig. 29 but from 1150 to 1167 Å. The remaining discrepancies are attributed to interstellar lines of CO not included in the interstellar spectrum synthesis.

of radiation driven winds is applicable even in such an extreme case.

As pointed out by Kudritzki (1992), the observed value of V_∞ can be used to determine the actual stellar mass using the theory of radiation driven winds, because for a given $T_{\rm eff}$ and R the terminal velocity is a strong function of the stellar mass. Fig. 33 shows the application to the case of HD 93129A. We obtain a mass of $130 \pm 15\ M_\odot$ corresponding to a gravity of 3.97 ± 0.05. This means that the masses derived from $\log g$ and V_∞ are consistent.

Very recently, Puls et al. (1996) in their study of O-star winds reported a systematic defect of the theory of radiation driven winds in the sense that for objects of very high luminosity with dense winds the theory does not provide enough wind momentum flow ($\dot{M}\ V_\infty$) when compared with the observation. It may, therefore, be surprising that in the case of HD 93129A the agreement is almost perfect. However, inspection of Figs. 26a and 29 in Puls et al. indicates that the discrepancy is less severe for very hot stars. In particular for HD 93129A Puls et al. assuming $T_{\rm eff}$=50500K obtain a theoretical wind momentum of only 0.2 dex too small. Now with new atomic data especially for iron the observed $\dot{M}$ is 20% smaller. In addition, with $T_{\rm eff}$=52000K the luminosity is somewhat higher yielding a slightly higher theoretical wind momentum so that the discrepancy disappears. We think that a similar study like this one for other early O-supergiants will be extremely valuable for a further investigation of the reliability of the theory.

5. Discussion

Following Simon et al. (1983) we can determine the stellar radius of HD 93129A from the distance to the Carina nebula, the effective temperature and the de−reddened magnitude. We obtain $R/R_\odot$=19.7. Together with $T_{\rm eff}$=52000 K this leads to a luminosity of $\log L/L_\odot$=6.4 with an uncertainty of 0.1 dex resulting from photometry, distance and effective temperature (see Simon et al.). HD 93129A is therefore the most luminous star known in our galaxy. From its location in the HR-diagram (see Fig. 34) we conclude that its Zero Age Main Sequence mass must have been slightly in excess of 120 $M_\odot$. Its present mass determined from gravity and V_∞ (see Sect. 4) is in agreement with this value. Despite the fact that HD 93129A has not yet lost a substantial amount of its mass our abundance analysis shows that the atmosphere is already enriched with products of CNO cycle material. We attribute this to additional mixing processes (Langer & Maeder, 1995). All other abundances appear to be solar.

The extreme dynamical wind properties, an extremely high rate of mass-loss together with a very high value of the terminal velocity can be well explained by the theory of radiation driven winds. While this extremely luminous object fits well into the present concept of stellar winds, its shock emission properties do not. Contrary, to the case of ζ Puppis, where cool and high temperature shocks contributed equally to the X-ray emission, the contribution of cooler shocks is much weaker for HD 93129A. This is not understood at the moment and we plan the analysis of FUV and X-spectra of a larger sample of O-stars to investigation this question further.

Acknowledgements. This work was supported by DARA under grant WE 2 - 50 QV 94019 - ZA, DFG under grant Ku 474/16-1, Pa 477/1-2, BMFT under grant 010R9008 and NASA grant NAG5-696. The ORFEUS-1 program is supported by DARA grant WE 3 - 50 OB 8501 3. The calculations have been carried out on the Cray YMP 4/32 of the Bayerische Akademie der Wissenschaften. We wish to thank M. Lennon for help in the atomic data, F. Sellmaier for calculating stellar wind models with EUV blocking included and S. Becker for providing Fe II atomic data.

Appendix A: effective, realization of the Sobolev approach including continuum processes

The work published in this Sect. is part of the diploma thesis by G. Taresch and was developed in collaboration with J. Puls.

A crucial quantity in the Sobolev approximation for spherical extended atmospheres is the so called "core penetration probability", generalized for an angle-dependent continuum radiation field.

$$\overline{\beta_C\, I_C} \;=\; \frac{1}{2}\int_{-1}^{1} I^{cont}(\nu_0(1+\frac{\mu\, v(r)}{c}),\mu)\;\frac{1-e^{-\tau_S}}{\tau_S}\;d\mu \tag{A1}$$

We have developed an approximate, very effective and fairly accurate method to calculate this quantity in order to avoid the time consuming angular integrations required to solve A1.

Expanding the intensity linearly in μ (which is the angle between the light ray and the outward radial direction) within the three ranges $1 \rightarrow \mu_*, \mu_* \rightarrow 0$ and $0 \rightarrow -1$ ($\mu_* = (1 - (R_*/r)^{1/2})$ we have

$$I_\nu(\mu) \;=\; a^1_\nu + b^1_\nu\,\mu, \qquad \mu_* \le \mu \le 1$$
$$I_\nu(\mu) \;=\; a^2_\nu + b^2_\nu\,\mu, \qquad 0 \le \mu < \mu_*$$

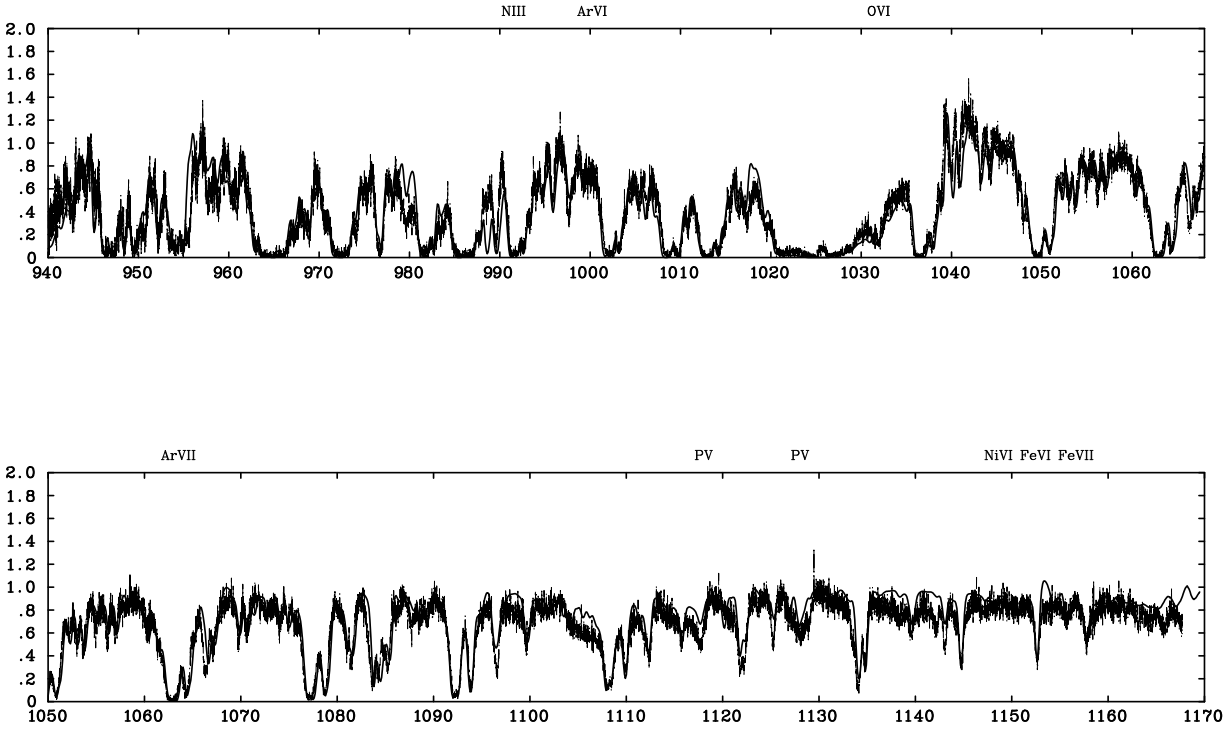

Fig. 31. The ORFEUS spectrum of HD 93129A (dash-dotted) compared with our final model (solid)

$$I_\nu(\mu) \;=\; a_\nu^3 + b_\nu^3\,\mu, \qquad\qquad -1 \le \mu < 0 \tag{A2}$$

Assuming that $a_\nu^i \approx a_{\nu_0}^i$ and $b_\nu^i \approx b_{\nu_0}^i$, the integral in A1 can be split into

$$\begin{aligned}\overline{\beta_C\, I_C} \;\approx\; & \frac{1}{2}\sum_{i=1}^{3} a_\nu^i \int_{\mu_{i+1}}^{\mu} \frac{1-e^{-\tau_S}}{\tau_S} d\mu \\ & + \frac{1}{2}\sum_{i=1}^{3} b_\nu^i \int_{\mu_{i+1}}^{\mu} \frac{1-e^{-\tau_S}}{\tau_S}\mu d\mu \end{aligned} \tag{A3}$$

with $\mu_1 = 1$, $\mu_2 = \mu_*$, $\mu_3 = 0$ and $\mu_4 = -1$.

The coefficients a_ν^i and b_ν^i are derived by combining the moments of the of the intensity J_ν, H_ν, K_ν and N_ν which are known from solving the continuum radiative transfer, e.g.

$$J_\nu = \frac{1}{2}\sum_{i=1}^{3} \int_{\mu_{i+1}}^{\mu} \left(a_\nu^i + b_\nu^i\,\mu\right) d\mu \tag{A4}$$

.

We find

$$\begin{aligned} a_\nu^1 &= 3\,J + 12\,H\,da_1 - 6\,K - 20\,N\,da_1 \\ a_\nu^2 &= 3\,J - 12\,H\,da_2 - 6\,K + 20\,N\,da_2 \\ a_\nu^3 &= a_\nu^2 \\ b_\nu^1 &= -4\,J + 3\,H\,(1-db_1) + 12\,K + 5\,N\,db_1 \\ b_\nu^2 &= \frac{a_\nu^1 - a_\nu^2}{\mu_*} + b_\nu^1 \\ b_\nu^3 &= 4\,J + 3\,H\,(1-db_2) - 12\,K + 5\,N\,db_2 \end{aligned} \tag{A5}$$

with

$$\begin{aligned} da_1 &= \frac{1+\frac{1}{2}\mu_*\left(3-{\mu_*}^2\right)}{\left(1-{\mu_*}^2\right)^2} \\ da_2 &= \frac{1-\frac{1}{2}\mu_*\left(3-{\mu_*}^2\right)}{\left(1-{\mu_*}^2\right)^2} \\ db_1 &= \frac{2\left(3-{\mu_*}^2\right)+4\mu_*\left(2-{\mu_*}^2\right)}{\left(1-{\mu_*}^2\right)^2} \\ db_2 &= \frac{2\left(3-{\mu_*}^2\right)-4\mu_*\left(2-{\mu_*}^2\right)}{\left(1-{\mu_*}^2\right)^2} \end{aligned} \tag{A6}$$

Test calculations performed for a large set of different parameters have shown that approximation A3 instead of calculating the "exact" quantity A1 is accurate at least to the third figure.

The second quantity to be calculated additionally in the Sobolev plus continuum concept is the interaction function

$$\begin{aligned} & U(\tau_s, k_C/k'_L) = \\ & \tau_s \int_{-\infty}^{\infty} d\xi\,\Phi(\xi) \int_{\xi}^{\infty} d\xi'\,\Phi(\xi') \\ & exp\left(-\tau_s \int_{\xi}^{\xi'} \Phi(s)\,ds\right)\left(1 - exp\left(-\frac{k_C}{k'_L}\,\tau_s\,(\xi'-\xi)\right)\right) \end{aligned} \tag{A7}$$

introduced by Hummer & Rybicki (1985) ($k'_L = k_L/\Delta\,\nu_D$). For a pure Dopplerprofile $\Phi(\xi)$ and $\tau_s > 0$, it is tabulated by Puls

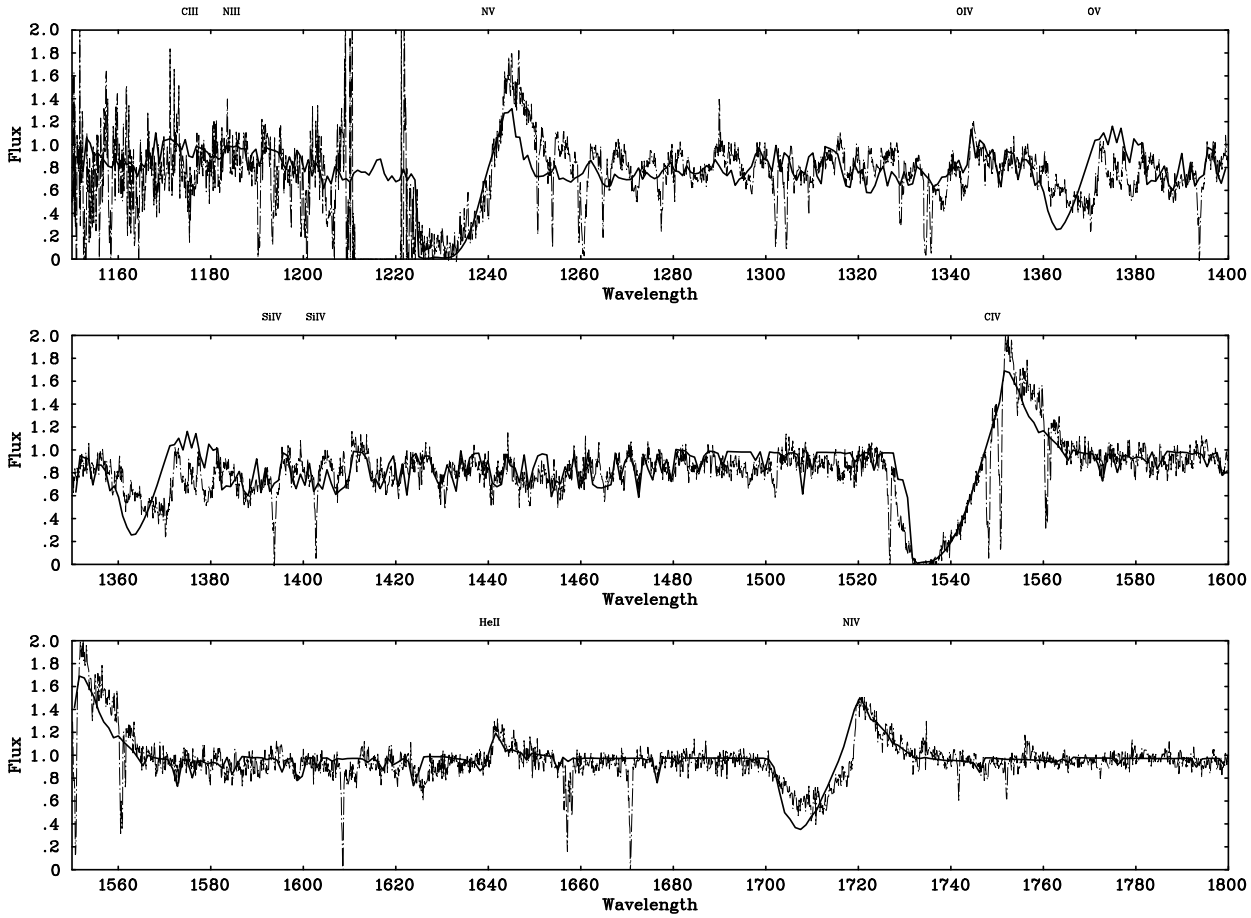

Fig. 32. The IUE spectrum of HD 93129A (dash-dotted) compared with our final model (solid)

& Hummer (1988) for $\frac{k_C}{k'_L} \leq 0.01$ and by Taresch (1992) for $10^{-10} \leq \frac{k_C}{k'_L} \leq 10^5$.

In the following, we provide some useful analytical approximations for two possible limiting cases.

i) $\tau_s >> 1$, i.e., the escape probability of the photons is very small ($\beta, \beta_c << 1$) which is typical for resonance lines in stellar atmospheres. Again, we have two limits, namely a dominating continuum ($k_C >> k'_L$) or a dominating line ($k_C << k'_L$).

For $k_C >> k'_L$, the interaction function can be approximated by

$$U = 1 \tag{A8}$$

and controls the mean intensity $\overline{J} \approx S_c$, as to be expected.

For $k_C << k'_L$, the influence of the interaction function is reduced to

$$U = 4k_C/k'_L \tag{A9}$$

and can be neglected for a thin continuum ($k_C \rightarrow 0$) when U reaches zero. Hence we achieve the standard Sobolev approach.

ii) $\tau_s << 1$, as is typical for recombination lines. Then, we find for a dominating continuum the limiting value

$$U = \frac{\tau_s}{2} - \frac{1}{\sqrt{2\pi}\, k_C/k'_L} \tag{A10}$$

For $k_C << k'_L$, e.g. in the outer stellar wind regions, the interaction function reaches

$$U = \frac{1}{\sqrt{2\pi}} \frac{k_C}{k'_L} \tau_s^2 \tag{A11}$$

which again can be neglected.

For inverted levels ($\tau_s < 0$, $\beta > 1$), the multiple integrals in the interaction function U will grow exponentially and we encounter numerical problems for a dominating continuum. To overcome these problems we split the U function in two parts:

$$\overline{U} = U_1 + U_2, \qquad U_1 = 1 - \beta, \qquad U_2 = \overline{U} - 1 + \beta \tag{A12}$$

Thus we find

$$U_2 = |\tau_s| \int_{-\infty}^{\infty} d\xi\, \Phi(\xi) \int_{\xi}^{\infty} d\xi'\, \Phi(\xi') \; exp\left(|\tau_s| \int_{\xi}^{\xi'} \Phi(s)\, ds - |\frac{k'_C}{k'_L}\, \tau_s| (\xi' - \xi) \right) \tag{A13}$$

which has the advantage to reach zero for $\frac{k_C}{k'_L} \rightarrow \infty$. For a dominating line ($k_C << k'_L$) it is approximated by $-(1-\beta)$ and U reaches zero. Thus we achieve again the standard Sobolev approach.

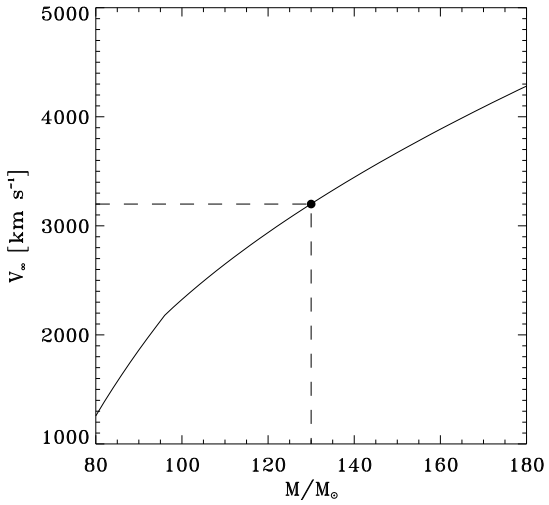

Fig. 33. V_∞ calculated as function of stellar mass for $T_{\rm eff}$=52000K and R=19.7 $R_\odot$using the theory of radiation driven winds with the force multiplier parameters as calculated in Sect. 4.

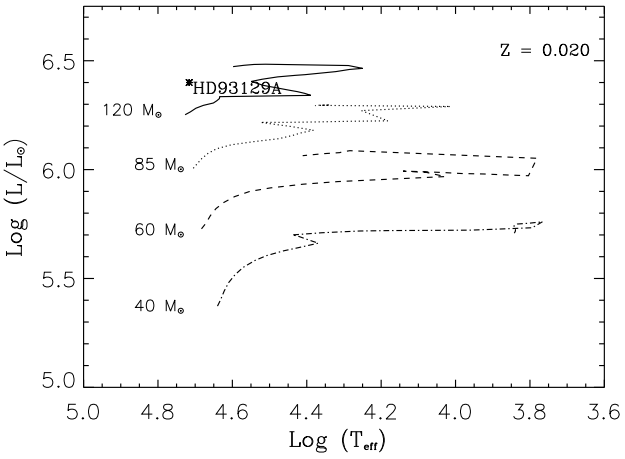

Fig. 34. Position of HD 93129A in the HR-diagram together with evolutionary tracks calculated by Schaller et al. (1992)

Following Puls & Hummer 1988, we have

$$\overline{\beta_C\, I_C} = \frac{1}{r}\int_0^r dz u(p,z)\frac{1-e^{-\tau_S(p,z)}}{\tau_S(p,z)} \quad \text{(A14)}$$

with the Feautrier variable $u(p,z) = 1/2(I^+(p,z) + I^-(p,z))$.

In order to avoid numerical difficulties for strong continua and $\beta > 1$, we reformulate this equation by

$$\overline{\beta_C\, I_C} = \frac{1}{r}\int_0^r (u(p,z) - S_c)\,\frac{1-e^{-\tau_S(p,z)}}{\tau_S(p,z)}dz + S_c\,\beta \quad \text{(A15)}$$

With this formulation, the radiative bound-bound coefficients of the reduced rate-equation read in the case of inverted lines

$$R_{ij} \;=\; B_{ij}\left(\frac{1}{r}\int_0^r (u(p,z) \;-\; S_c)\;\frac{1-e^{-\tau_S(p,z)}}{\tau_S(p,z)}\;dz\right) \quad \text{(A16)}$$

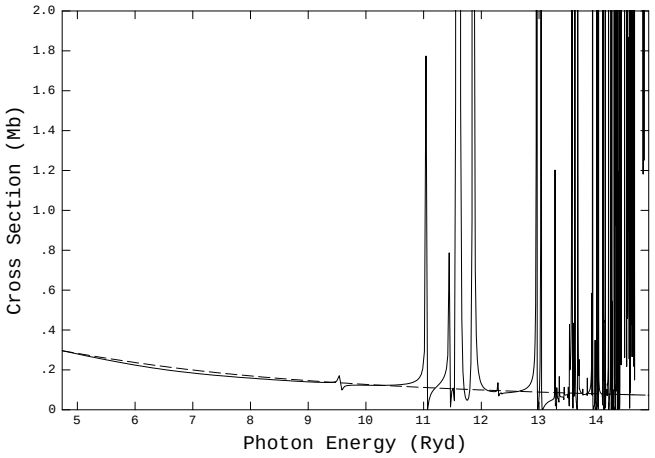

Fig. 35. Close coupling photoionization cross section (solid) compared with Seaton Fit for threshold α = 0.267 and β = 1.8 and S = 1.6 (dashed) for ground state of P V

$$\begin{aligned} &+B_{ij}\,(S_c(1\,+\,U_2)) \\ R_{ji} \;=\; &B_{ji}\left(\frac{1}{r}\int_0^1 (u(p,z)\;-\;S_c)\;\frac{1-e^{-\tau_S(p,z)}}{\tau_S(p,z)}\;dz\right) \\ &+B_{ji}\,(S_c(1\,+\,U_2)) + A_{ji}(1\,+\,U_2) \end{aligned} \quad \text{(A17)}$$

with the obvious limits

$$R_{ij} \;=\; B_{ij}\;S_c \quad \text{(A18)}$$

$$R_{ji} \;=\; B_{ji}\;S_c + A_{ji} \quad \text{(A19)}$$

for dominating continua, consistent with Eq. (A8).

Appendix B: the Phosphorus atomic model and the P V resonance line

The formation of the P V resonance line strongly depends on ionization and recombination processes. Thus, to ensure that the ionization structure of Phosphorus is optimally reproduced within the scope of our models we improved our atomic model.

The resulting values are given in Table 8.

While the energy levels and transition probabilities calculated with SUPERSTRUCTURE (Eissner et al. 1974) are satisfactory (see PKPBH) we had to improve the photoionization data as differences with cross sections calculated using the close coupling method were obvious. The new close coupling data for P VI, P V and P IV were were fitted by a polynomial, to derive the threshold value α and β and S given in the Seaton formula).

Hunsinger (1993) suggested that K-shell absorption could be important for stars much hotter than ζ Puppis. Thus we improved our model by introducing this absorption for Phosphorus for HD 93129A. The threshold energy E_t, the threshold value of the cross section $\sigma_t = \frac{\sigma_0}{1.3}$, the parameter S and the effective charge are calculated following Daltabuit & Cox (1972), the resulting values are given in Table 9 together with the number of electrons N.

Table 8. Photoionization cross section P IV, P Vand P VI (Seaton)

P IV-State	α	β	S	P V-State	α	β	S	P VI-State	α	β	S
3s ^{1}S	0.647	1.2	1.7	3s ^{2}S	0.296	1.80	1.60	2p^6 ^{1}S	3.28	3.20	3.10
3p ^{3}P^o	0.487	3.0	1.2	3p ^{2}P^o	0.557	2.13	2.00	3s ^{3}P^o	0.260	2.50	2.00
3p ^{1}P^o	0.214	3.5	0.2	3d ^{2}D	1.28	0.01	2.30	3s ^{1}P^o	0.253	2.50	2.30
3d ^{1}D	1.82	1.5	2.0	4s ^{2}S	0.387	1.68	1.80	3p ^{3}S	0.446	2.50	2.10
3p^2 ^{3}P	0.20	0.2	2.3	4p ^{2}P^o	0.611	1.94	1.80	3p ^{3}D	0.477	2.50	2.30
3p^2 ^{3}P	0.80	2.6	1.5	4d ^{2}D	2.30	2.06	3.30	3p ^{1}P	0.426	2.50	2.20
3d ^{3}D	2.6	0.4	2.0	4f ^{2}F^o	1.19	2.00	4.30	3p ^{3}P	0.485	2.50	2.30
3p^2 ^{1}S	0.152	0.2	3.0	5s ^{2}S	0.558	1.55	1.90	3p ^{1}D	0.473	2.50	2.20
3p^2 ^{1}S	0.63	2.6	1.0	5p ^{2}P^o	0.830	1.30	1.60	3p ^{1}S	0.629	2.50	2.40
3d ^{1}D	3.17	0.7	2.0	5d ^{2}D	3.70	1.59	2.70	3d ^{3}P^o	0.856	1.00	3.10
4s ^{3}S	0.631	0.4	0.9	5f ^{2}F^o	2.94	1.60	3.50	3d ^{3}F^o	0.874	0.70	3.00
4s ^{1}S	0.571	1.5	2.0	6s ^{2}S	0.780	1.70	2.00	3d ^{1}F^o	0.832	0.70	3.00
4p ^{3}P^o	0.404	2.2	1.2	6p ^{2}P^o	1.18	1.00	1.55	3d ^{1}D^o	0.833	0.70	3.00
4p ^{1}P^o	0.368	3.0	1.2	6d ^{2}D	5.64	2.00	2.80	3d ^{3}D^o	0.832	0.70	3.00
3d ^{1}D^o	0.40	0.3	2.5	6f ^{2}F^o	5.47	2.00	3.35				
3d ^{1}D^o	2.2	1.3	2.0	7s ^{2}S	1.11	1.30	1.75				
3d ^{1}F^o	9.67	0.3	2.1	7p ^{2}P^o	1.80	1.00	1.65				
3d ^{3}P^o	0.848	0.5	2.5	7d ^{2}D	8.71	1.00	2.20				
3d ^{3}P^o	2.67	0.6	2.3	7f ^{2}F^o	9.47	1.00	2.50				
3d ^{3}D^o	0.20	1.5	2.0								
3d ^{3}D^o	3.17	0.8	2.3								
4d ^{3}D	5.28	0.3	1.9								
4d ^{1}D	7.95	0.3	2.1								
3d ^{1}P^o	1.5	0.3	2.1								
3d ^{1}P^o	3.2	0.5	2.2								

Table 9. K-shell photoionization cross section parameters for Phosphorus

N	$E_{th}[eV]$	$\sigma_0[10^{-18}\,cm^2]$	S	Z_{eff}
3	2666.	0.111	2.89	13.94
4	2571.	0.115	2.88	13.67
5	2500.	0.118	2.88	13.47
6	2443.	0.121	2.87	13.30
7	2396.	0.123	2.87	13.17
8	2357.	0.125	2.86	13.05
9	2322.	0.127	2.86	12.95
10	2291.	0.129	2.86	12.85
11	2264.	0.130	2.86	12.77
12	2240.	0.132	2.85	12.70
13	2217.	0.133	2.85	12.63
14	2197.	0.134	2.85	12.57
15	2178.	0.135	2.85	12.51

It turned out, that for HD 93129A, showing an effective temperature of 52000 K, K-shell absorption is negligible, as there is no difference between models calculated with or without this effect.

References

Allison A.C., Dalgarno A., 1970, Atomic Data, 1, 289
Conti P.S., Frost S.A., 1977, ApJ, 212, 728
Cox D.P., Raymond J.C., 1985, ApJ, 298, 651
Dabrowski I., Herzberg G., 1974, CJP, 52, 1110
Dabrowski I., Herzberg G., 1975, CJP, 54, 525
Dalgarno A., Black J.H., Weisheit J.C., 1973, ApJL, 14, 77
Daltabuit E., Cox D.P., 1972, ApJ, 177, 855
Davenhall C., 1977, "UCL internal memo, Everything you wanted to know about the new CoG program but were afraid to ask."
Eissner W., Jones M., Nussbaumer H., 1974, Comput. Phys. Commun., 8, 270
Feldmeier A., Kudritzki R.P., Palsa R., Pauldrach A.W.A., Puls J., 1996, A&A, submitted
Groenewegen M.A.T., Lamers H.J.G.L.M., 1989, A&AS, 79, 359
Hamann W.-R., 1981, A&A, 93, 353
Haser S., 1995, PhD Thesis, Munich
Haser S.M., Lennon D.J., Kudritzki R.-P., et al., 1995, A&A, 295, 136
Henrichs H.F., 1991, in D. Baade, ed., Rapid Variability of OB Stars: Nature and Diagnostic Value, ESO Conference and Workshop proceedings No.36: Munich
Herrero A., 1994, Space Science Reviews, 66, 137
Herrero A., Kudritzki R.P., Vilchez J.M., et al., 1992, A&A, 261, 209
Hillier D.J., Kudritzki R.P., Pauldrach A.W., et al., 1993, A&A, 276, 117

Howarth I.D., Prinja R.K., 1989, ApJ, 69, 527
Hummer D.G., Rybicki G.B., 1985, ApJ, 293, 258
Hunsinger J., 1993, Diploma Thesis, Munich
Hurwitz M., Bowyer S., 1991, in Extreme Ultraviolet Astronomy, ed. S. Bowyer & R.F. Malina (New York:Pergamon), 442
Jenkins E.B., Jura M., Loewenstein M., 1983, ApJ, 270, 88
Jura M., 1975a, ApJ, 197, 575
Jura M., 1975b, ApJ, 197, 581
Jura M., York D.G., 1978, ApJ, 219, 861
Krämer G., Mandel H., 1993, ORFEUS-SPAS, Sterne und Weltraum, 32, 508
Krämer G., et al., 1990 in "Observatories in Earth Orbit and Beyond" (Proc. IAU Colloquium 123), Y. Kondo ed., Kluwer Publ., Dordrecht 1990, p. 177
Kudritzki R.P., 1980, A&A, 85, 174
Kudritzki R.P., 1992, A&A, 266, 395
Kudritzki R.P., Hummer D.G., 1990, Ann. Rev A&A, 28, 303
Kudritzki R.P., Palsa R., Feldmeier A., Puls J., Pauldrach A.W.A., 1996, in: Zimmermann H.U., Trümper J., Yorke H. (eds.), Röntgenstrahlung from the Universe, MPE Report 263, Garching, p. 9
Lamers H.J.G.L.M., Cerruti-Sola M., Perinotto M., 1987, ApJ, 314, 726
Langer N., Maeder A., 1995, A&A, 295, 685
Lucy L.B., 1982, ApJ, 255, 268
Lucy L.B., 1983, ApJ, 274, 374
Mihalas D., Hummer D.G., 1973, ApJ, 179, 827
Moffat 1978, A&A, 68,41
Morton D.C., 1975, ApJ, 197,85
Morton D.C., 1991, ApJS, 77, 119
Morton D.C., Dinerstein H.L., 1976, ApJ, 204, 1
Morton D.C., Hu E.M., 1975, ApJ, 202, 638
Morton D.C., Noreau L., 1994, ApJS, 95, 301
Pauldrach A.W.A., Kudritzki R.P., Puls J., Butler K., Hunsinger J., 1994, A&A, 283, 525 (PKPBH)
Pauldrach A.W.A., Feldmeier A., Puls J., Kudritzki R.P., 1994b, Space Science Reviews, 66, 105
Puls J., 1991, A&A, 248, 581
Puls J., Hummer D.G., 1988, A&A, 191, 87
Puls J., Owocki S.P., Fullerton A.W., 1993, A&A, 279, 457
Puls J., Kudritzki R.P., Hererro A., et al., 1996, A&A, 305, 171
Raymond J.C., 1988, in: Pallavinci R. (ed.) Hot Thin Plasma in Astrophysics. Kluwer, Dortrecht, p. 3
Raymond J.C., Smith B.W., 1987, ApJS, 35, 419
Schaller G., Schaerer D., Meynet G., Maeder A., 1992, A&AS, 96, 269
Sellmaier F., 1996, PhD Thesis, Munich
Sellmaier F.H., Yamamoto T., Pauldrach A.W.A., Rubin R.H., 1996, A&A, in press
Shull J.M., York D.G., 1977, ApJ, 211, 803
Simon K.P., Jonas G., Kudritzki R.P., Rahe, J., 1983, A&A, 125, 34
Spitzer L., 1975, "Interstellar Matter Research with the Copernicus Satellite", in: Mitteilungen der Astronomischen Gesellschaft Nr. 38, p.27
Spitzer L., Cochran W.D., 1973, ApJ, 186, 23
Spitzer L., Zweibel E.G., 1974, ApJL, 191, L127
Spitzer L., Drake J.F., Jenkins E.B. et al. 1973, ApJ, 181, L116
Spitzer L., Cochran W.D., Hirshfeld A., 1974, ApJS, 28, 373
Strömgren B., 1948, ApJ, 108, 242
Taresch G., 1992, Diploma Thesis, Munich
Walborn N.R., 1971, ApJ, 167, L31
Walborn N.R., Nichols-Bohlin J., 1987, PASP, 99, 40
Walborn N.R., Heckathorn J.N., Hesser J.E., 1984, ApJ, 276, 524
York D.G., Spitzer L., Bohlin R.C., et al., 1983, ApJ, 266, L55

This article was processed by the author using Springer-Verlag LaTeX A&A style file *L-AA* version 3.